T. MILNE

EFFECTS OF PRESSURE ON BIOMASS PYROLYSIS AND GASIFICATION

William S. Mok

Michael J. Antal, Jr. (P.I.)

Final S.E.R.I. Report

November 1981

DEPARTMENT OF MECHANICAL AND AEROSPACE ENGINEERING

PRINCETON UNIVERSITY

PRINCETON, NEW JERSEY 08544

TABLE OF CONTENTS

LIST OF TABLES

LIST OF ILLUSTRATIONS

ABSTRACT

Results of research using a tubular, laminar flow, micro reactor system to explore the effects of pressure on the products of biomass pyrolysis and partial oxidation, and the heats of pyrolysis of various biomass materials are described in this paper. In general, increasing pressure increases the yields of char, CO_2 and H_2, and decreases the yields of CO, CH_4, C_2H_4, C_2H_6 and C_3H_6. The addition of small amounts of O_2 reduces the yields of all hydrocarbons, but has no effect on char formation. Increasing pressure has a dramatic effect on the heats of pyrolysis of biomass materials, changing the sign of $\Delta H_{pyrolysis}$ from positive (endothermic) to negative (exothermic). These results furnish important fundamental data for use by the designers of biomass gasification reactors.

1.0 INTRODUCTION

The techniques of thermal analysis have been skillfully developed by scientists interested in the thermal properties of synthetic and natural polymers. Unfortunately, these techniques have not been extensively applied to studies of the thermal properties of biomass materials. The primary objective of this research effort has been to utilize a tubular micro reactor system embedded in a Setaram Differential Scanning Calorimeter (DSC) to explore the effects of pressure on the products and heats of pyrolysis of cellulose, the primary component of most biomass materials. A secondary objective has been to develop improved techniques for detailing the mechanisms and kinetics of the solid phase pyrolysis of various biomass materials using non-isothermal thermogravimetry. The long range goal of this research is to develop detailed mechanistic and kinetic models which mathematically account for the effects of heating rate and final temperature, gaseous environment and pressure, particle size, etc. on the behavior of biomass materials in a pyrolytic environment.

2.0 THERMAL ANALYSIS OF VARIOUS ORGANIC MATERIALS

The primary emphasis of the past year in the area of thermal analysis has been the development of numerical techniques for interpreting the complex solid phase mechanisms and kinetics evidenced during the solid phase pyrolysis of biomass materials. Preliminary results of this research have been published (see Reference 1 and Appendix A), and a comprehensive paper is being prepared (2). Research described in Reference 3 (see Appendix B) evidences the utility of this work.

Some experimental work was accomplished (see Sections 2.2 and 2.3) using the DuPont 951 Thermal Analysis System and the Setaram DSC. Unfortunately, the DuPont instrument is unable to provide sufficiently accurate temperature measurements (see Appendix B) to permit the acquisition of reliable kinetic data. Experimental results and their interpretation are discussed in the following sections.

2.1 Apparatus and Experimental Procedures

A detailed explanation of the apparatus and experimental procedures is given in Appendix B.

2.2 Results

TG, DTG and Friedman curves for Avicel PH102 cellulose, levoglucosan, Indulin AT Kraft lignin, and ground corn cob material are given in Figures 1-4 (cellulose), 5-8 (levoglucosan), 9-12 (lignin), and 13-16 (corn cob).

2.3 Discussion of Results

The Friedman curves for cellulose (Figures 3 and 4) are clear signatures of the reaction mechanism

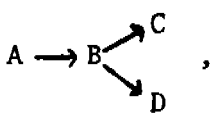

,

confirming the low temperature work of Broido and Shafizadeh. The influence of crystallinity is also evident in this work in comparison with earlier work at Princeton. However, there is also clear evidence for additional pyrolytic phenomena early on in the reaction sequence which has not been elucidated by earlier workers.

The DTG (Figure 6) and Friedman curves (Figures 7 and 8) of levoglucosan are less easily interpreted. The major weight loss step appears to be a simple A→B mechanism from the DTG curve, but the Friedman curve indicates more strucure (accompanied by a high level of noise). The secondary, high temperature step

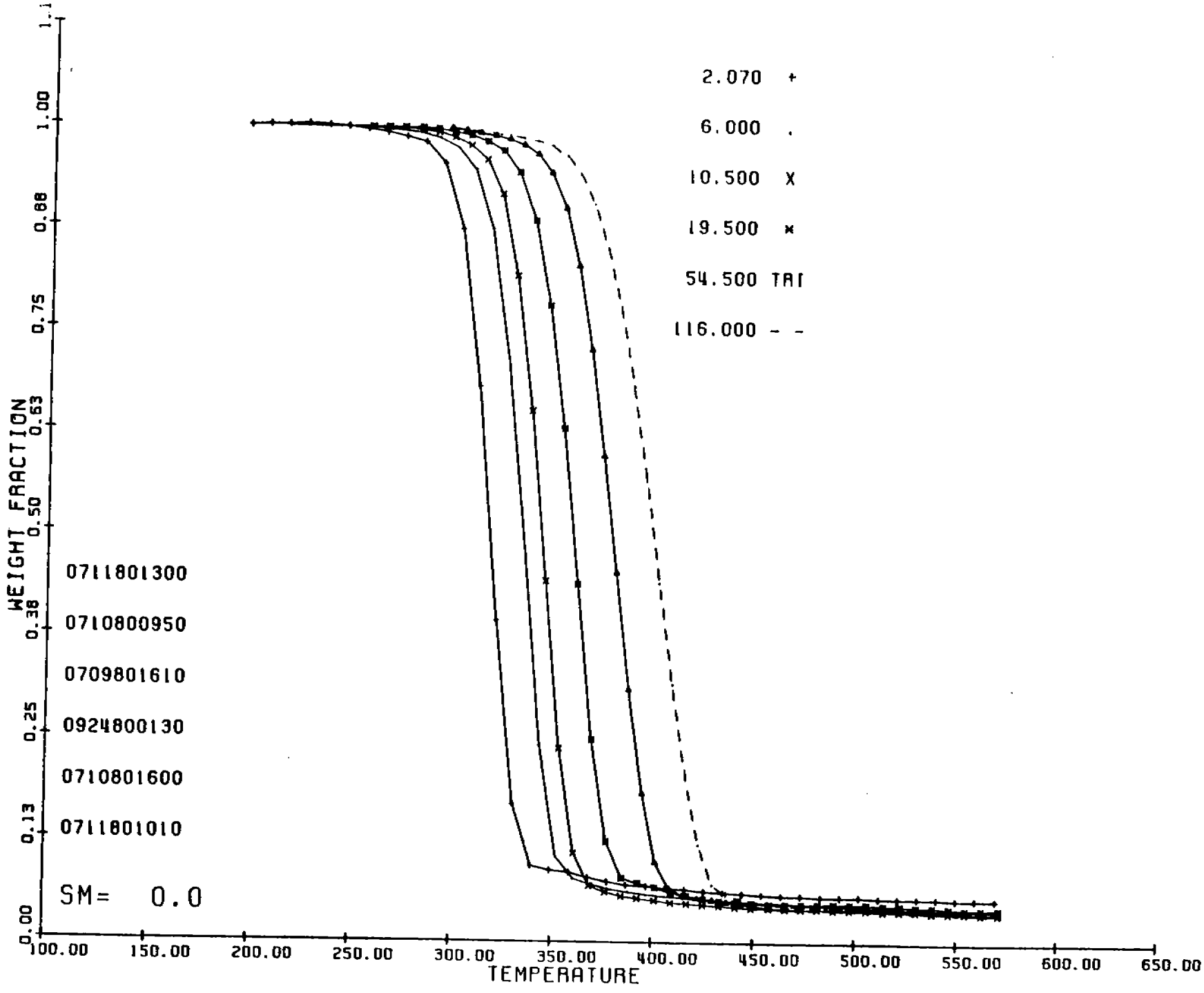

PH102 ALL 6 WT FRAC VS TEMPERATURE

Figure 1. TG Curves of Avicel PH102 Microcrystalline Cellulose

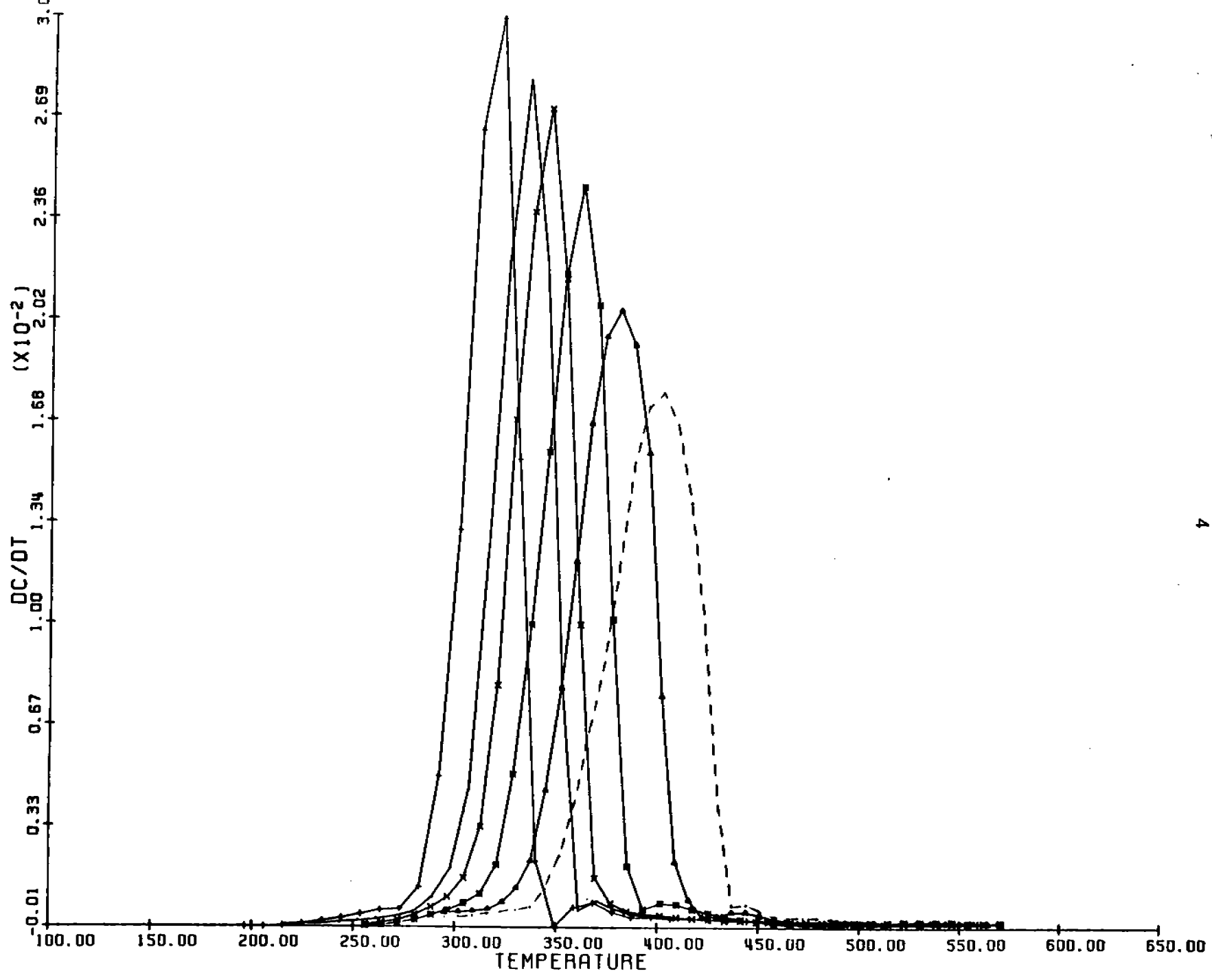

Figure 2. DTG Curves of Avicel PH102 Microcrystalline Cellulose

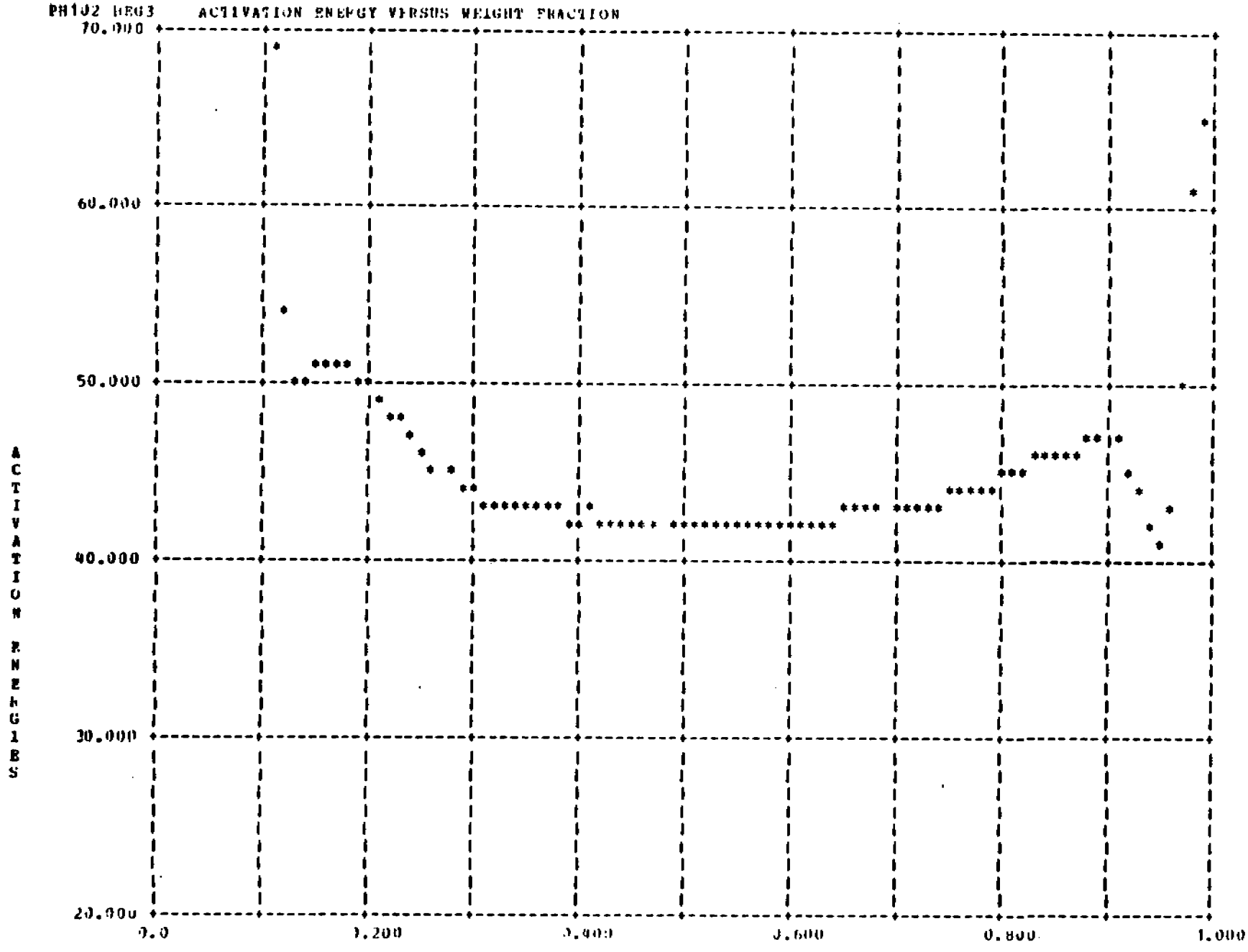

Figure 3. Low Heating Rate Friedman Curves of Avicel PH102 Microcrystalline Cellulose

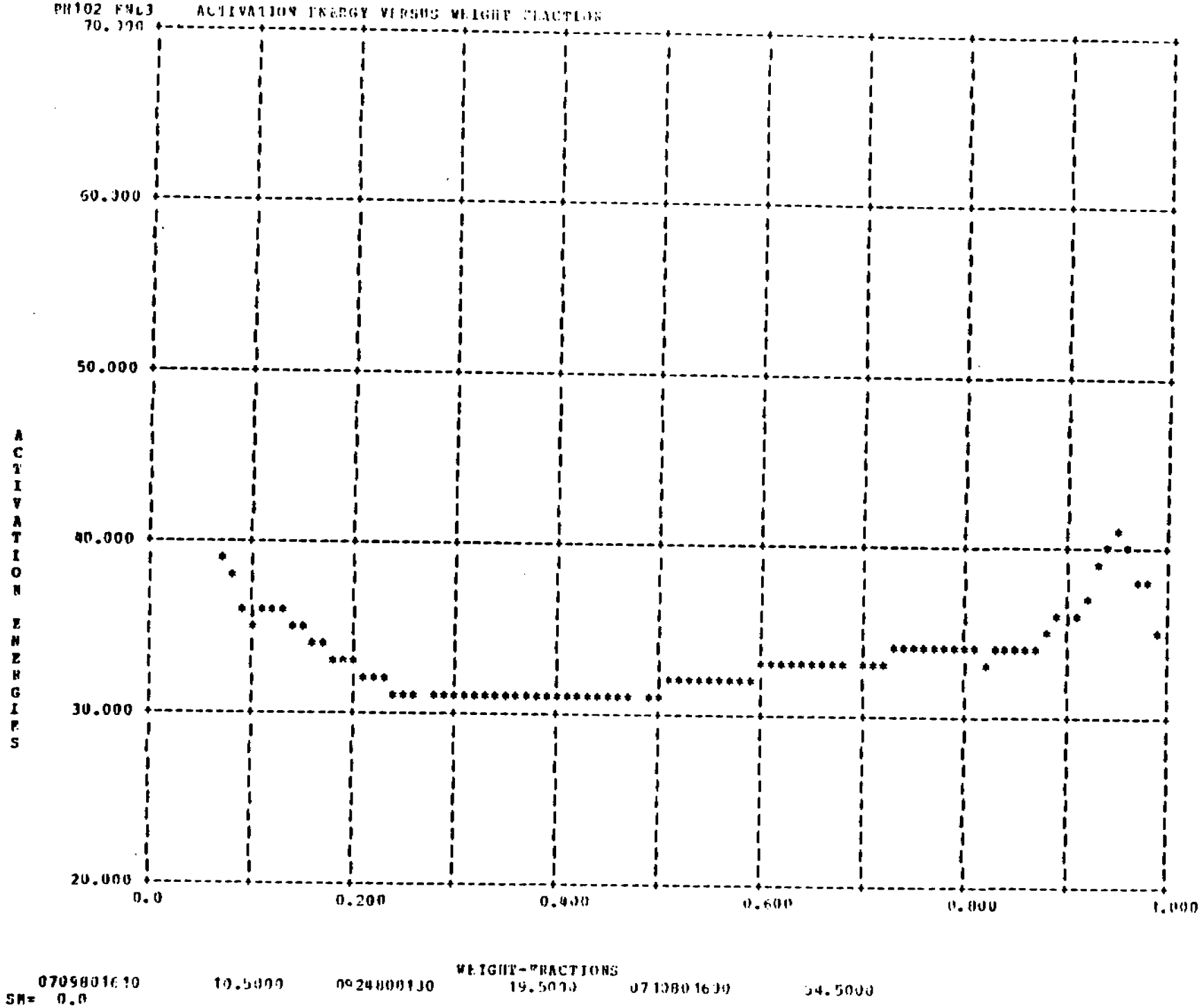

Figure 4. High Heating Rate Friedman Curves of Avicel PH102 Microcrystalline Cellulose

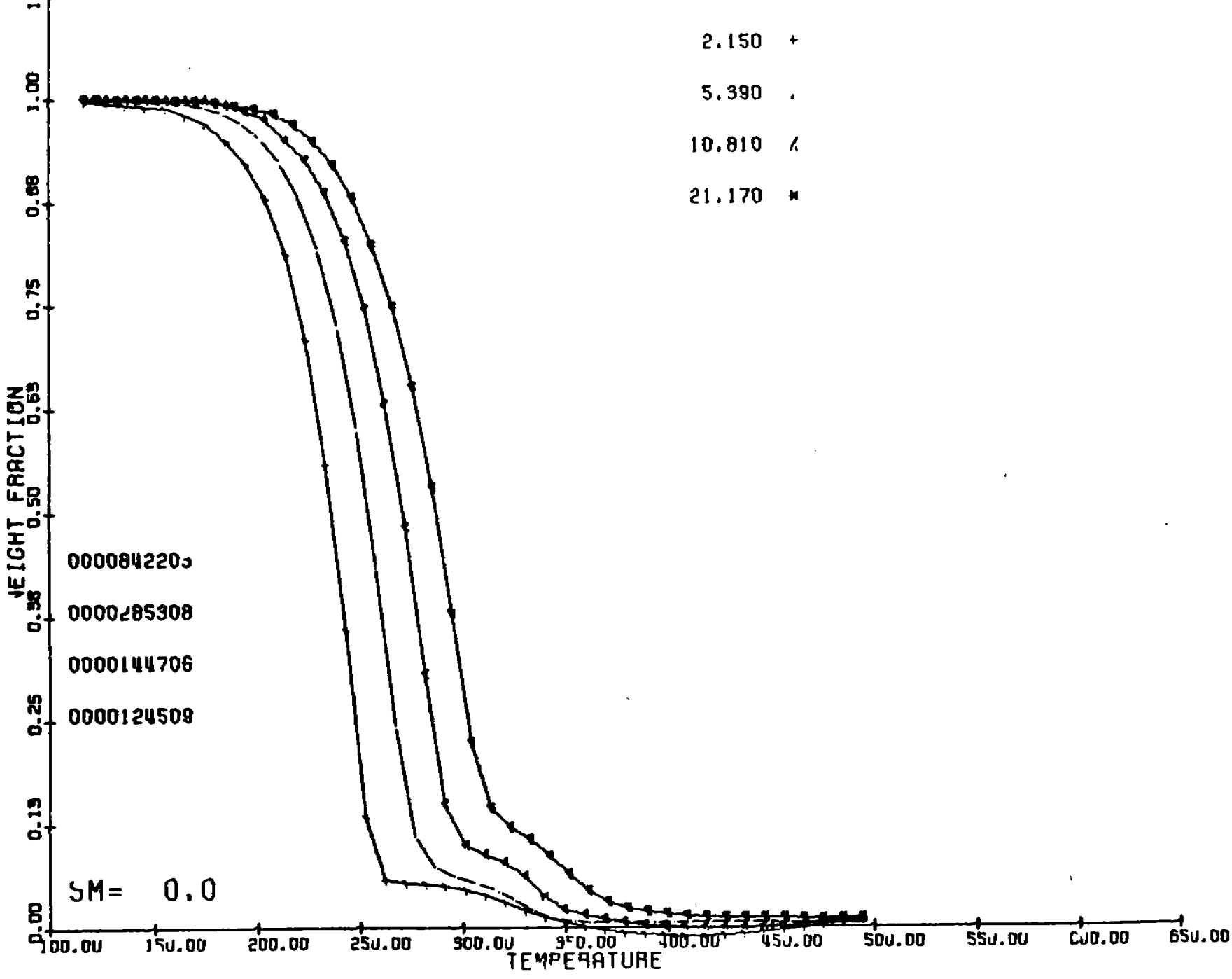

LEVO ALL 4 WI FRAC VS TEMPERATURE

Figure 5. TG Curves of Levoglucosan

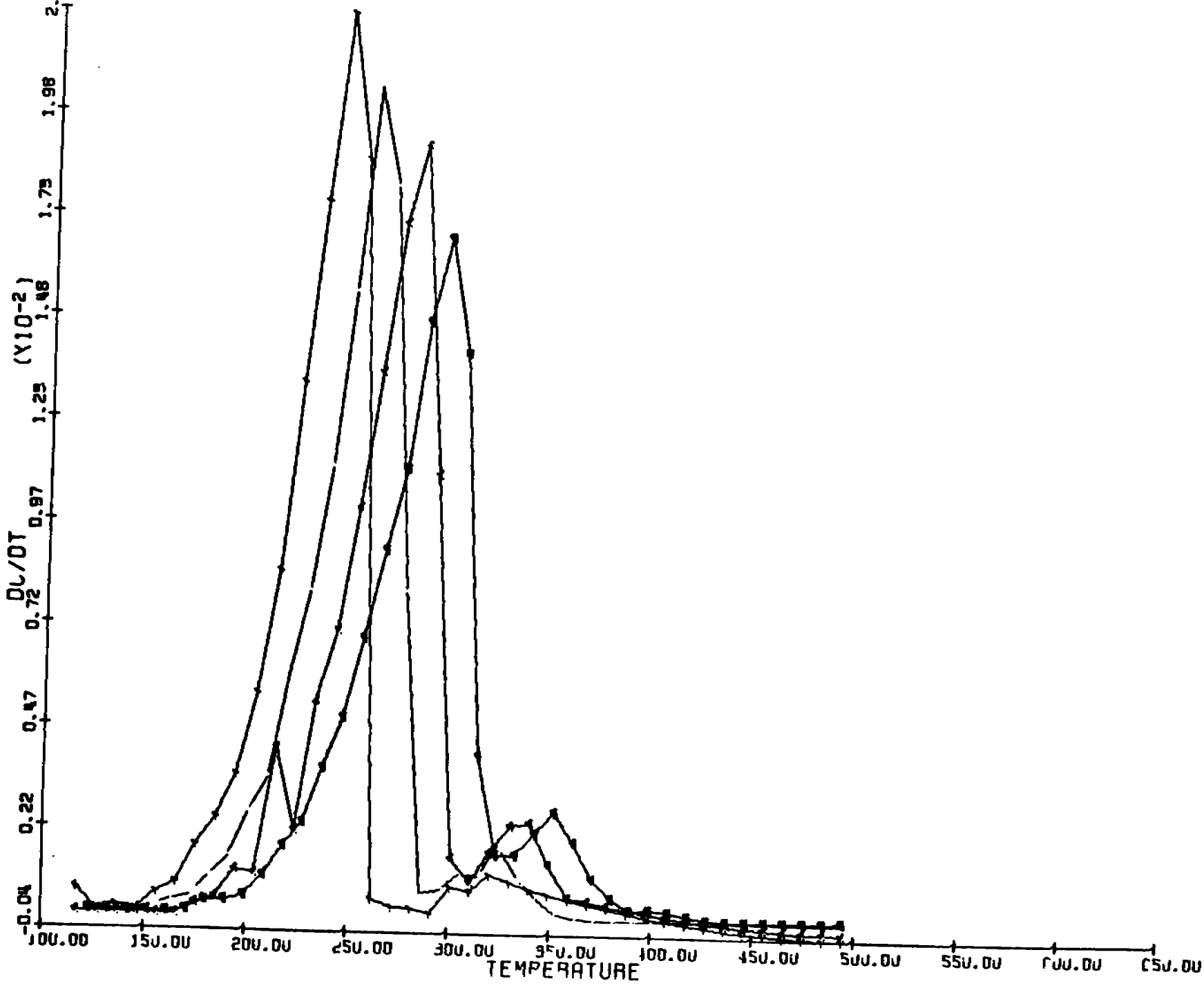

LEVO ALL 4 DC/DT VS TEMPERATURE

Figure 6. DTG Curves of Levoglucosan

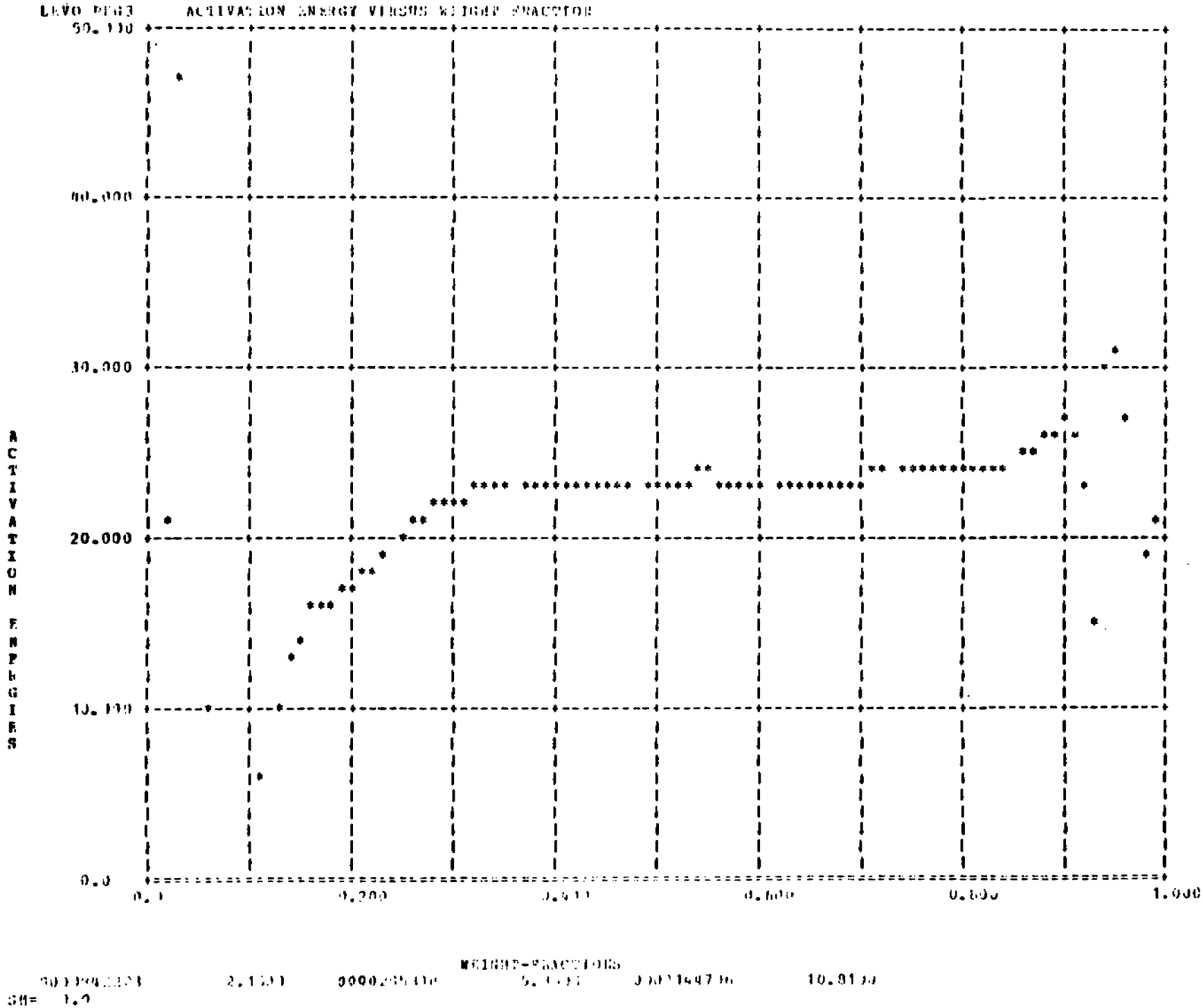

Figure 7. Low Heating Rate Friedman Curves of Levoglucosan

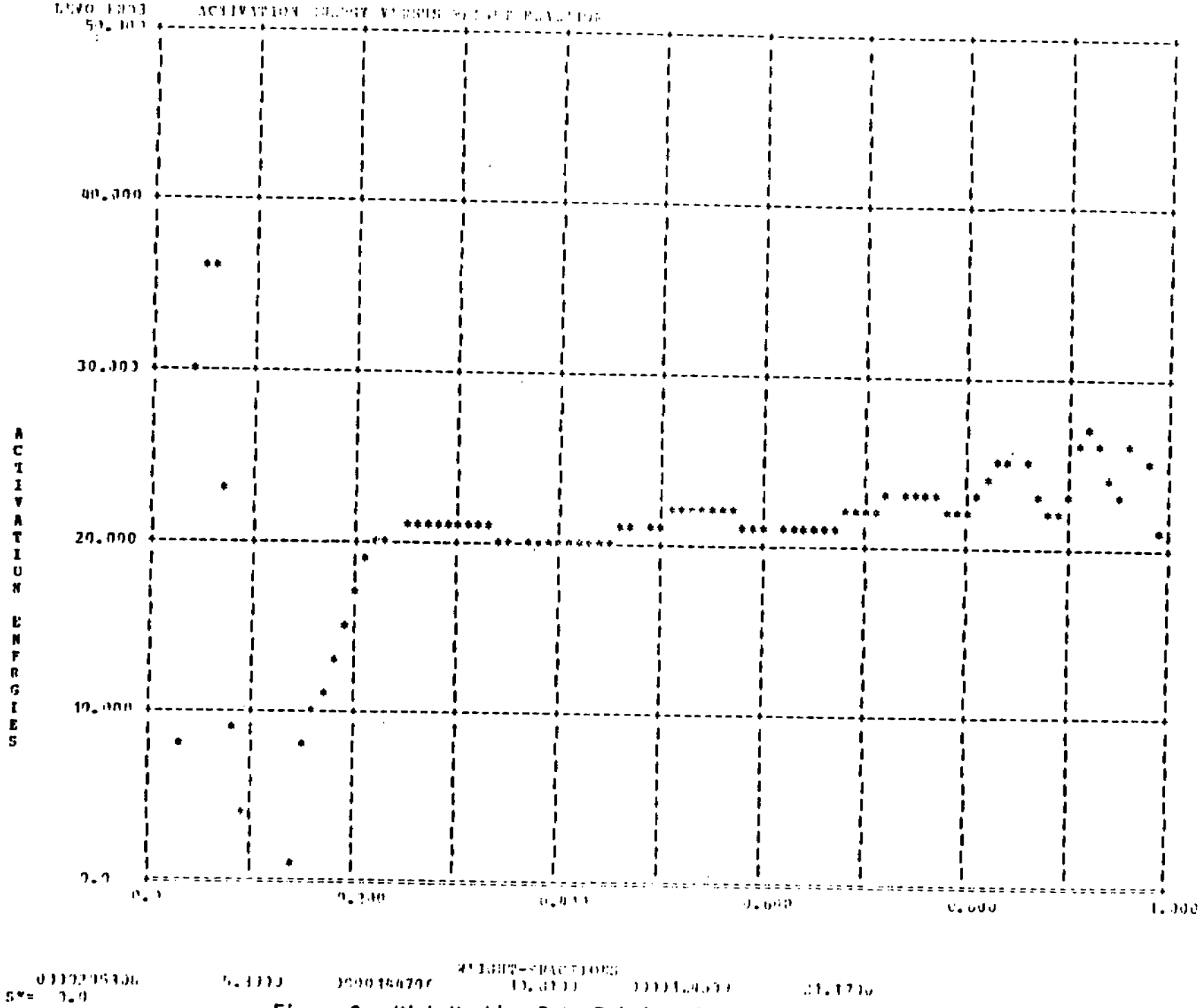

Figure 8. High Heating Rate Friedman Curves of Levoglucosan

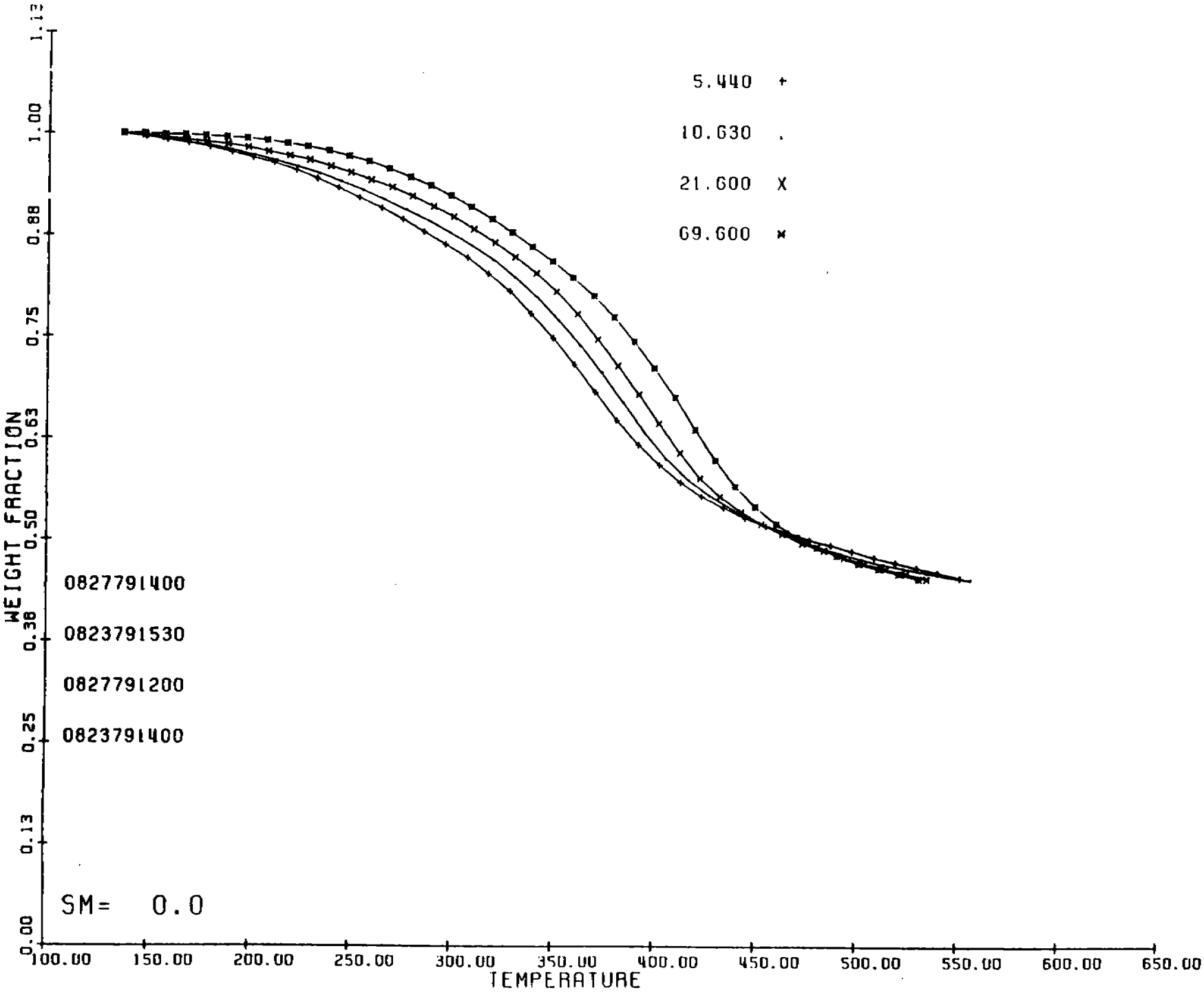

Figure 9. TG Curves of Indulin AT Kraft Lignin

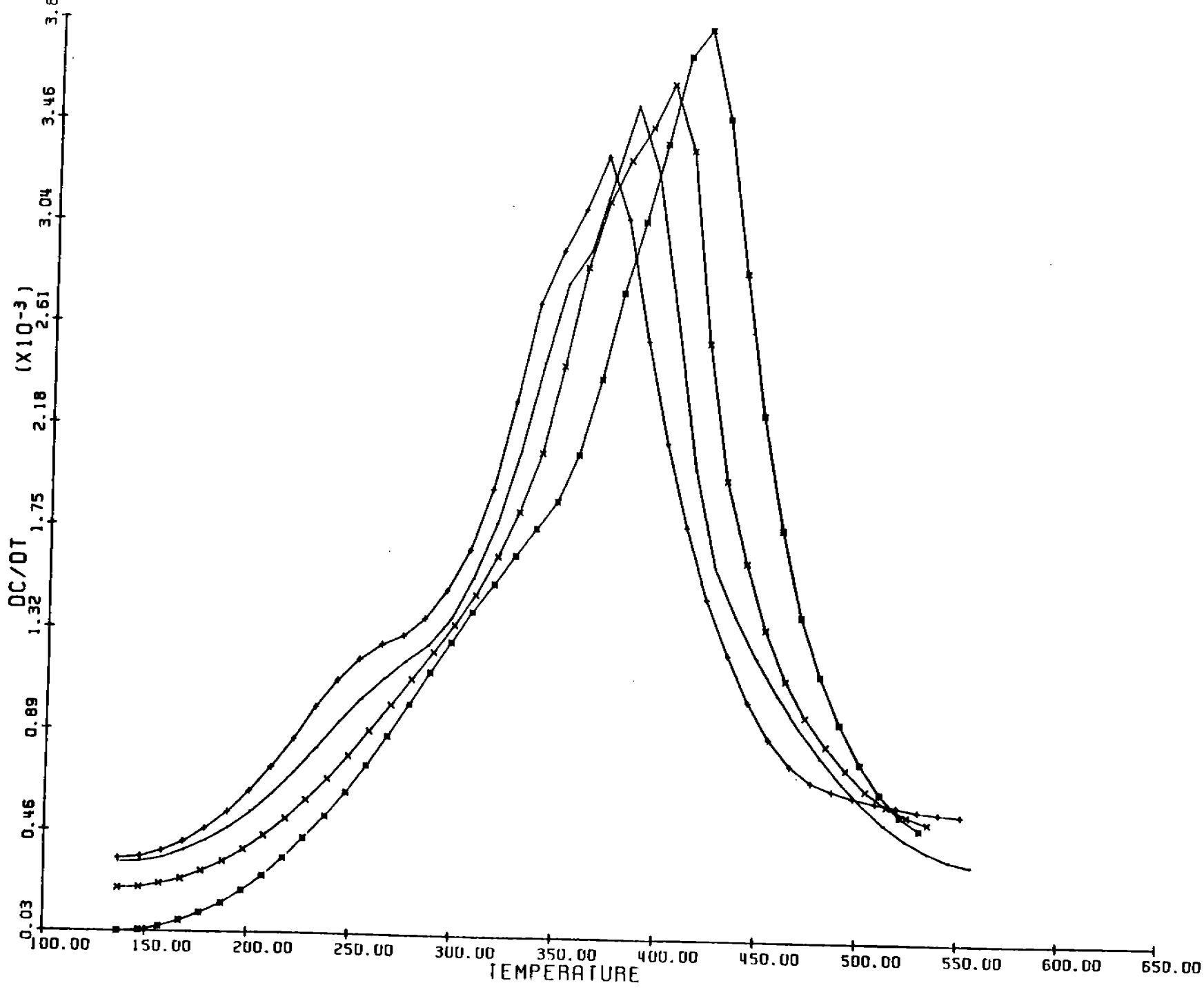

Figure 10. DTG Curves of Indulin AT Kraft Lignin

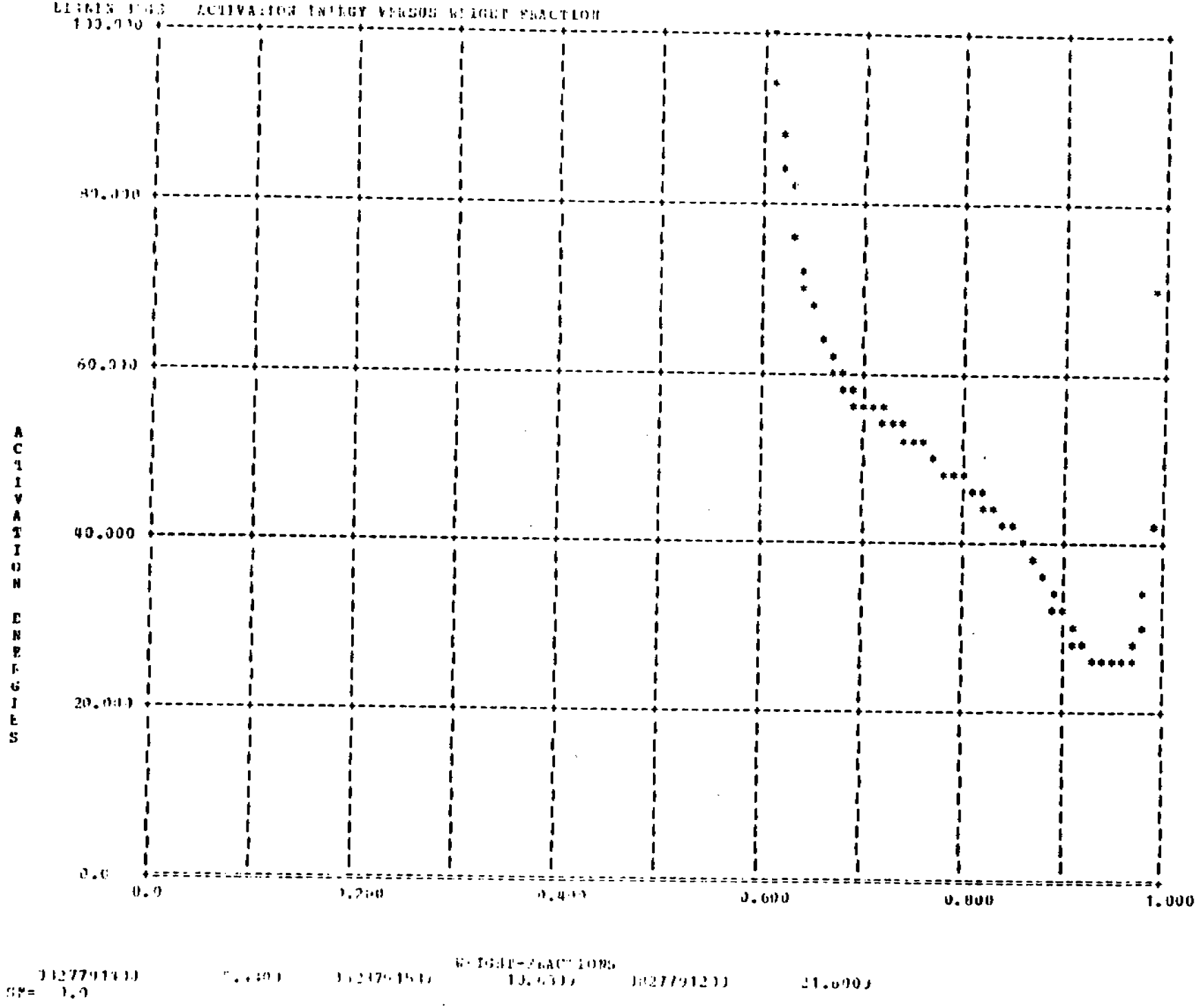

Figure 11. Low Heating Rate Friedman Curves of Indulin AT Kraft Lignin

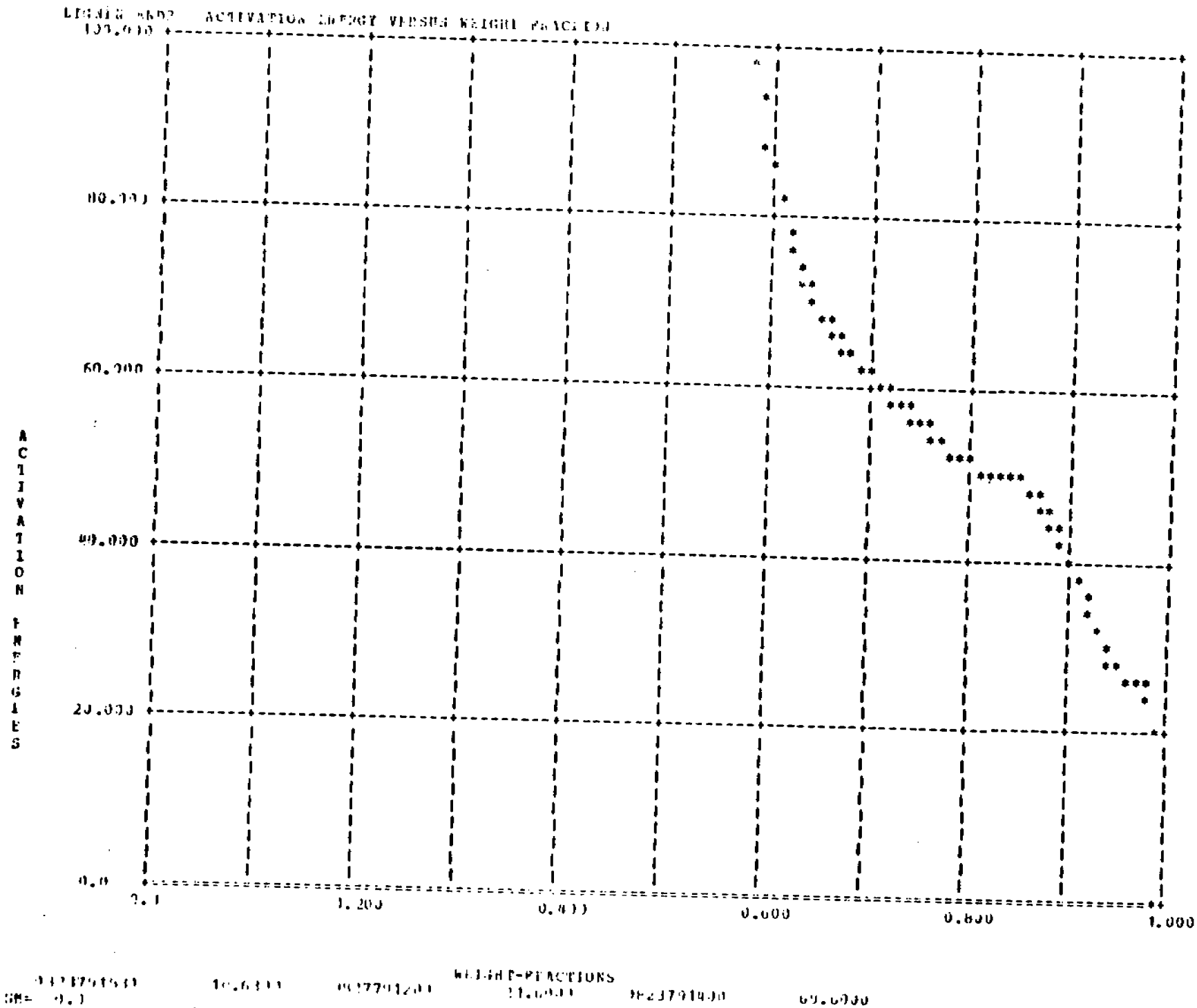

Figure 12. High Heating Rate Friedman Curves of Indulin AT Kraft Lignin

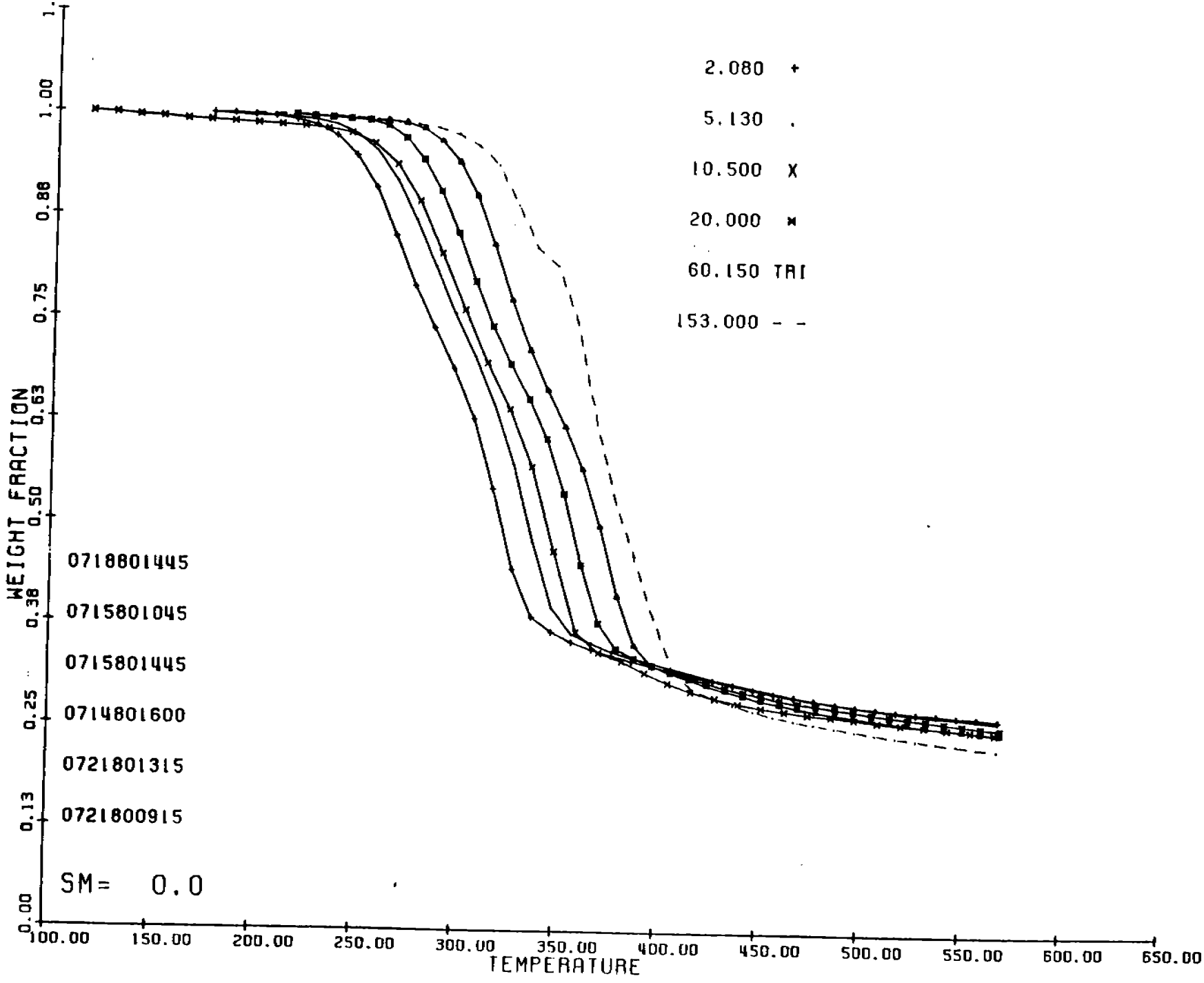

Figure 13. TG Curves of Ground Corncob Material

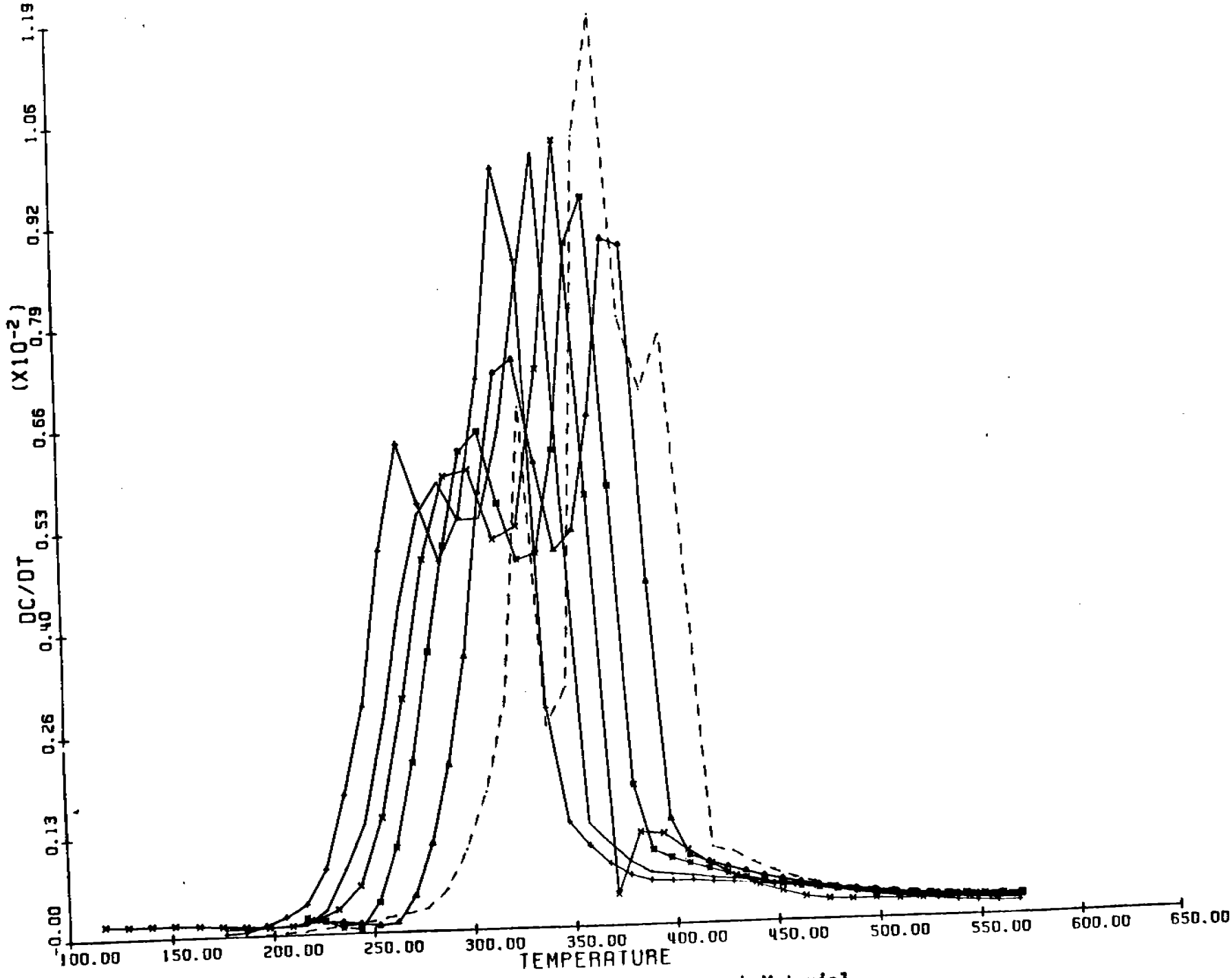

Figure 14. DTG Curves of Ground Corncob Material

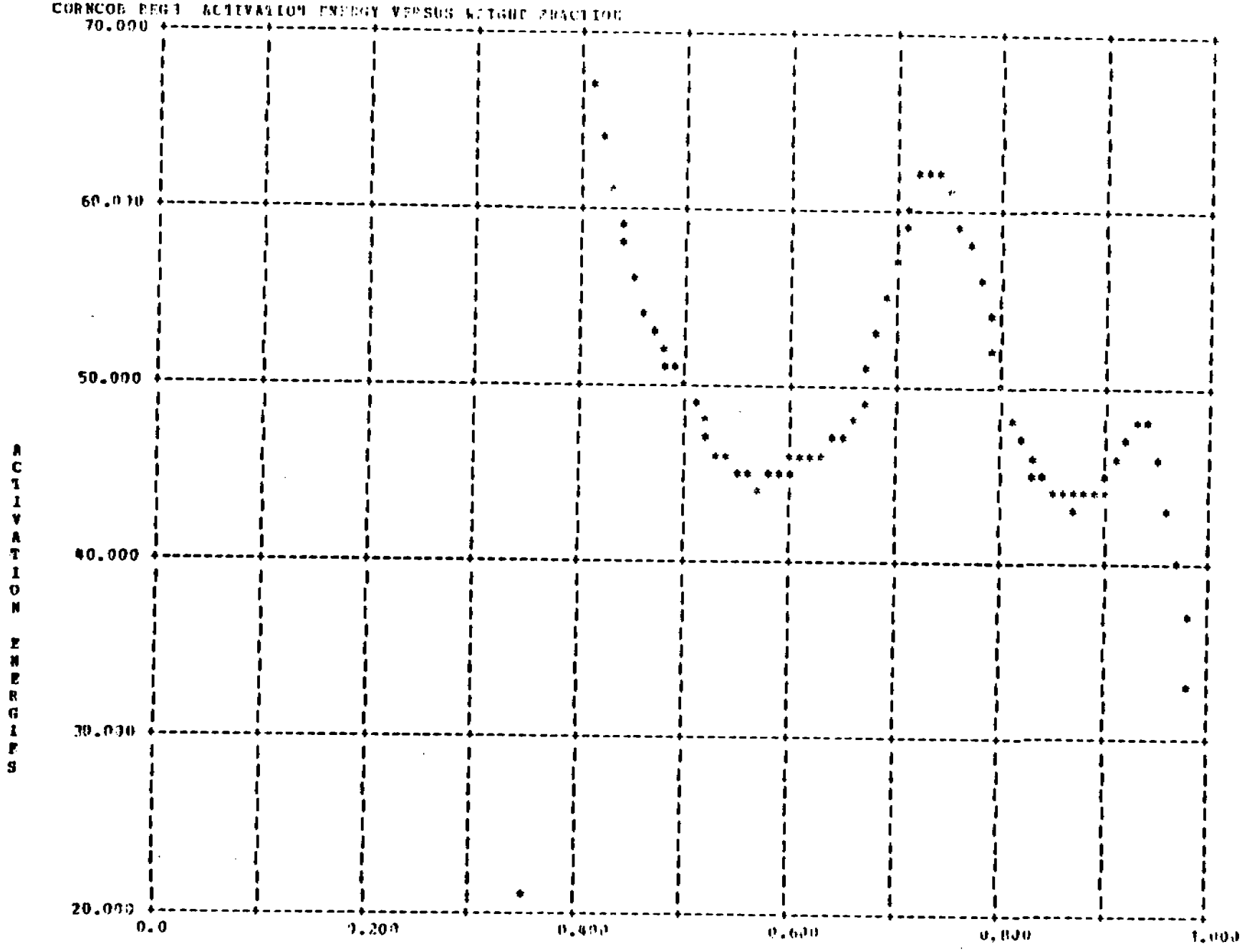

Figure 15. Low Heating Rate Friedman Curves of Ground Corncob Material

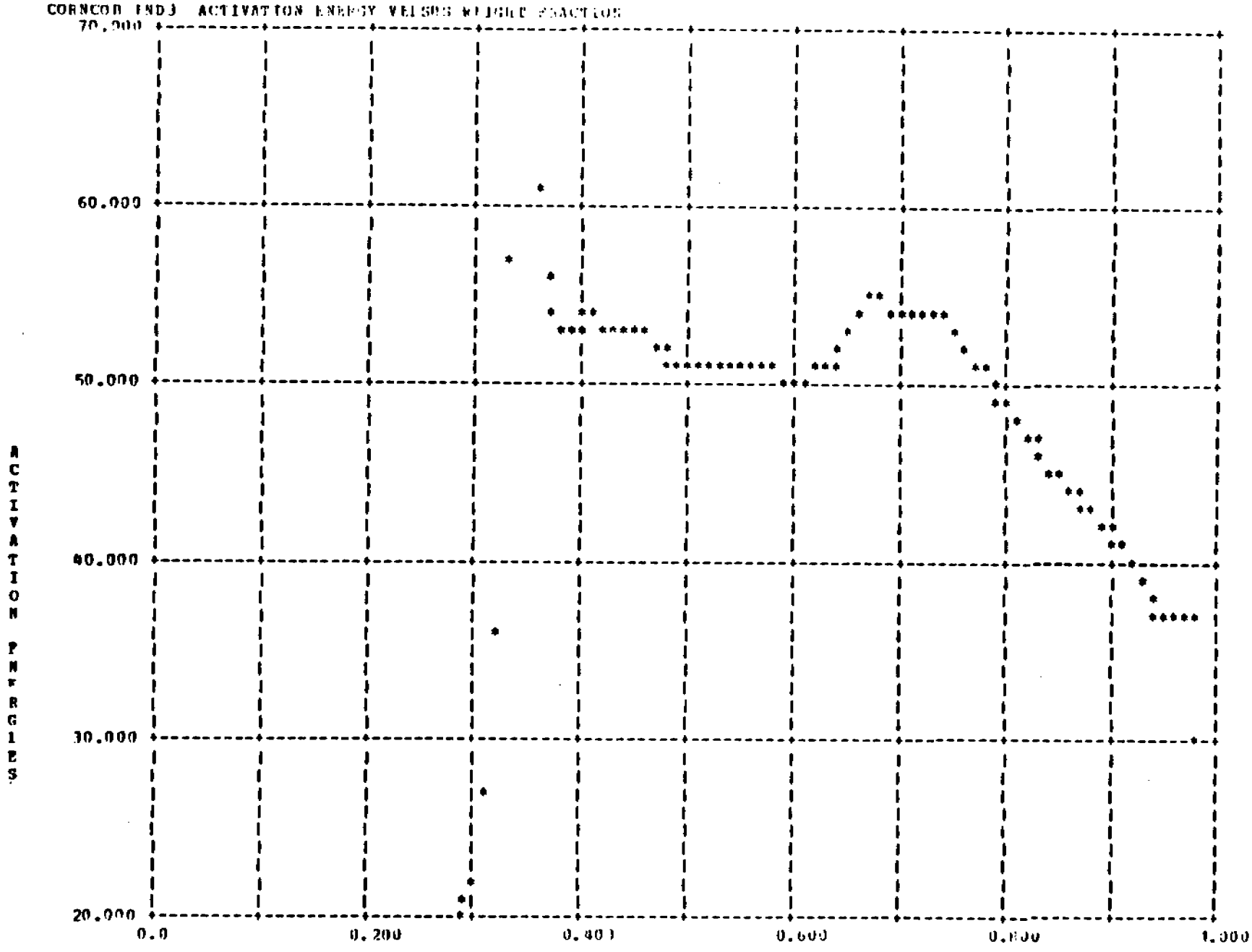

Figure 16. High Heating Rate Friedman Curves of Ground Corncob Material

WEIGHT-FRACTIONS

0715801445 10.5000 0714001600 20.0000 0721801315 60.1500

SN= 0.0

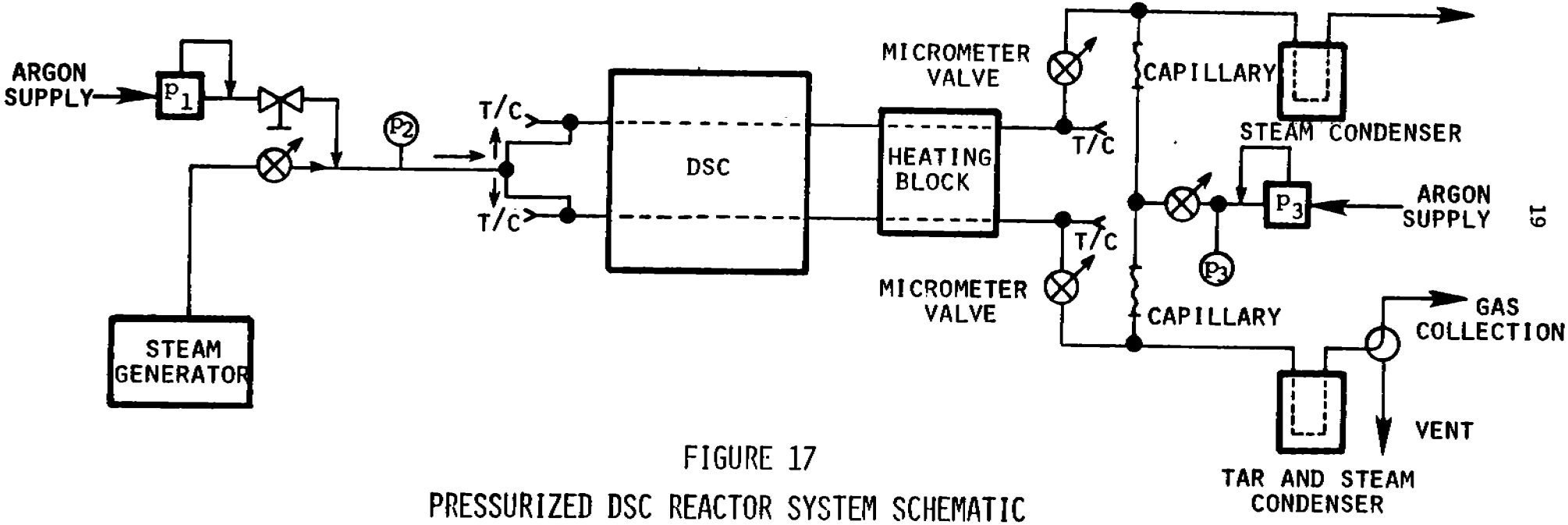

FIGURE 17

PRESSURIZED DSC REACTOR SYSTEM SCHEMATIC

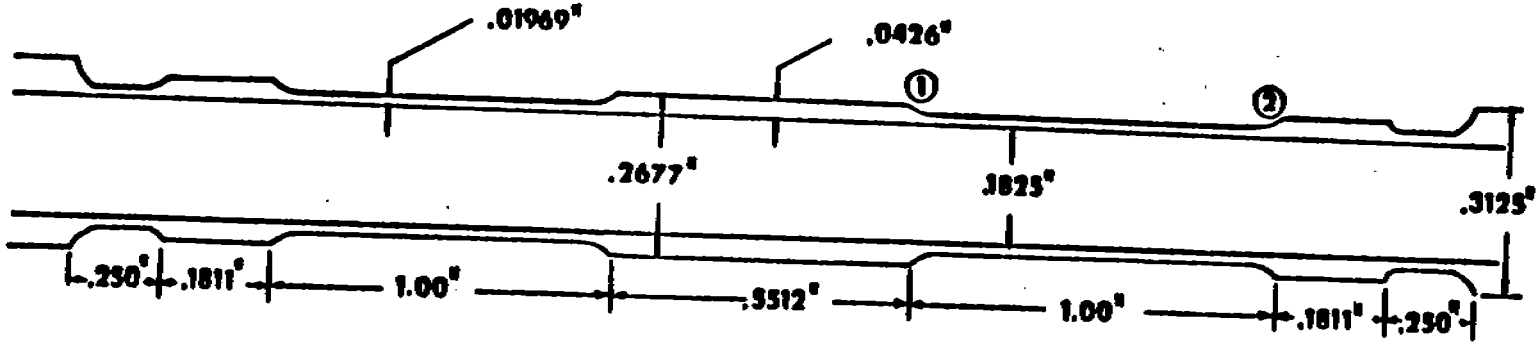

FIGURE 18

TUBULAR REACTOR SCHEMATIC

TABLE 1

THE SETARAM DIFFERENTIAL SCANNING CALORIMETER (DSC)

1. Is a calorimeter. It measures the *rate* of heat influx or outflow from a small reactor volume enclosed in a furnace.

2. Scans in temperature. It can heat the reactor volume from subambient to 827°C at heating rates up to 20°C/min.

3. Is actually two opposed calorimeters. It measures differences in heat flow between a control volume and a sample volume.

4. Is capable of "seeing" into a pressurized tubular steel reactor and reporting *rates* of chemical reactions occurring within it.

5. Is capable of measuring the total heat of reaction of the pyrolysis steam gasification process.

appears to be competitive from the DTG curve. The low activation energies associated with all these steps, and the downward shift of the Friedman curves with higher heating rates are clear evidence of diffusional phenomenon limiting the rate of weight loss.

Both the DTG (Figure 10) and the Friedman curves (Figures 11 and 12) for lignin are clear signatures of a competitive reaction $A \nearrow B$, $A \searrow C$. These signatures are so clear that the details of the mechanism could probably be unravelled by a senior as part of his BSE research.

Figures 13-16 detailing corn cob pyrolysis phenomena are extremely complex. Three parallel competitive reactions of the form $A_i \nearrow B_i$, $A_i \searrow C_i$ where i = 1,2, or 3 might simulate the weight loss phenomenon evidenced in Figures 13-16, but this is only a guess.

In all four cases considerably more work needs to be done to define the actual kinetic parameters and refine the mechanistic details sufficiently to provide a good mathematical description of the weight loss curves. Since the experimental results reflect the weaknesses of the DuPont TGA, it would probably be wise to direct future effort towards the acquisition of higher quality experimental data using a Setaram or Mettler TGA/DTA instrument before expending significant effort to model the results.

3.0 PRESSURIZED TUBULAR REACTOR EXPERIMENTS

This section details research accomplished during the past academic year (9/80 - 6/81) with the objective of studying the effects of pressure on cellulose pyrolysis. The work was broad in nature. It consisted of three phases:

1. A study of the effects of pressure, temperature and residence time on the overall pyrolysis product distribution, including primary solid phase pyrolysis products and subsequent gas phase cracking products. This work is the foundation for future studies of the pyrolytic gas phase chemistry.

2. A study of the effects of addition of a small amount of oxygen on cellulose pyrolysis. This part of the work has been exploratory in nature, paving the way to possible studies that will trace the chemical pathways leading to oxygen consumption. Mechanisms controlling CO vs CO_2 formation could possibly be detailed.
3. A study of the effects of pressure on the heat demand of the solid phase pyrolysis reactions. This work is very significant, not only in providing engineering data for reactor design, but also by offering improved insights into the cellulose pyrolysis mechanism; thereby contributing to the growing, yet not totally agreed upon, knowledge in solid phase pyrolysis of cellulose.

3.1 Apparatus

The design of the entire reactor system is depicted schematically in Figure 17. The most unique feature of this system is its inclusion of a Setaram Differential Scanning Calorimeter (DSC), capable of measuring the rates and heats of pyrolysis of the solid phase reactant. Table 1 details the various features of the DSC, and the role it plays in the reactor system.

Figure 18 is a schematic of the two micro-reactors, fabricated from type 316 stainless steel. These reactors were designed to provide: 1) reactor contact with the calorimeter sensor, 2) minimum lateral heat flux along the tube, and 3) the capability of repeated operation at 150 psi and 800°C. The reactor is zoned to enable separate study of solid phase (occurring in the DSC) and gas phase chemistry (occurring in the reactor zone surrounded by the heating block).

Steam was used only in the phase 1 and 2 experiments, when product gas collection was necessary. The Steam Master PP-6 steam generator is capable of providing pressure up to 6 atms, which set the upper pressure limit for this work.

However, in phase 3, argon was used as the purge gas, enabling a pressure up to 10 atms.

In phase 1, the reactor system was used without the DSC to facilitate the operation. The details of this simpler system are given in Figure 19. In stage 2, still without the DSC, the system was slightly modified to allow input of a small controlled amount of free oxygen. The system was then merged with the DSC, as in Figure 17, but with a tank of argon in place of the steam generator, for the phase 3 research.

3.2 Phase One Research

Phase 1 focused on the effects of pressure on pyrolysis products. Avicel PH102 microcrystalline cellulose samples were used in the initial experiments. The typical sample size, due to dimensional restrictions of the reactor, was on the order of 10 mg. This posed difficulties in handling, but minimized inter- and intra-particle heat transfer effects.

For all of the experiments conducted during this phase, zone A (Fig. 19), where the primary pyrolysis reaction takes place, was kept initially at 150°C and raised to 500°C in approximately four minutes. Zone B was kept isothermally at 700°C to effect the gas phase reactions. Tar collection was not possible with this set up; but from previous studies, tar formation was known to be minimal under the selected experimental condition. For most experiments, the gas phase residence time was set between 1 - 2 seconds.

3.2.1 Procedures. Calibrate the reactor to the desired pressure and residence time by simultaneously adjusting valve 1 and valve 2. Purge the air from the system. Insert sample. Connect condenser, start timing. Connect gas collector. Purge again with argon to drive air out. Start pyrolysis by heating zone A. Start product gas collection at 200°C. Analyze products by Gas Chromatography.

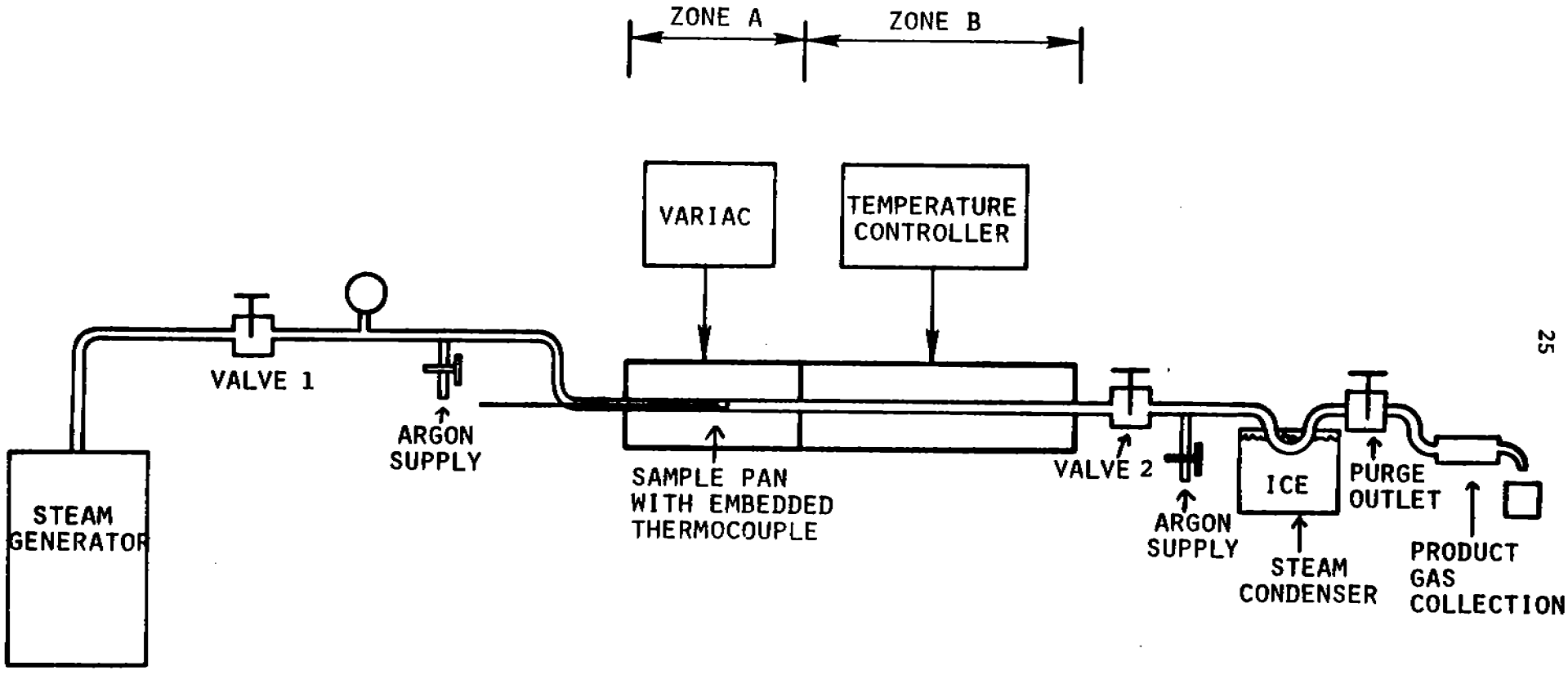

FIGURE 19: FLOW DIAGRAM FOR THE PRESSURIZED FLOW REACTOR (PHASE 1 EXPERIMENTS)

3.2.2 Results and Discussions. Experiments were first conducted at 1, 2 and 5 atm. More than one experiment was run at each pressure to check the repeatability of data. A 3 atm run was added to give a better picture of the trend of gas yields as a function of pressure.

The data collected evidences much scatter. This can be explained by noting some difficulties inherent in the experimental procedure. The setting of pressure and residence time was done by simultaneously adjusting valves 1 and 2 (Fig. 19), the effects of which couple with each other. Therefore it was difficult to set the reactor to the specific pressure desired while ensuring a residence time of 1 second (or some other predetermined value). Further, after the reactor was calibrated and the sample inserted, the heating of the solid phase pyrolysis zone changes the calibrated pressure, hence the residence time. The new pressure was reported by thepressure gauge, but the new residence time must be calculated using the amount of steam collected during the whole experimental period of operation. Therefore, while it was desired to have pressure as the only parameter, the effect of an accompanying change in residence time was difficult to avoid. Finally, the high surface area-to-volume ratio of the reactor could lead to various extraneous inconsistent wall effects. However, despite the scatter, we believe that the trends of gas yields shown are valid.

The findings can be summarized as follow (see Figures 20-23): as pressure increases, yields of CO, CH_4, C_2H_6, C_2H_4, C_3H_6 decrease; while yields of CO_2 and H_2 increase. Overall, the fraction of feed carbon and oxygen in the effluent gases decrease as pressure increases, while an increase of hydrogen fraction is detected.

Finally, an experiment was performed at 5 atms with an extended (10 secs) residence time. Based on previous studies (2), increased gas yields were found with increasing residence time up to about 1 sec. It was with the assumption

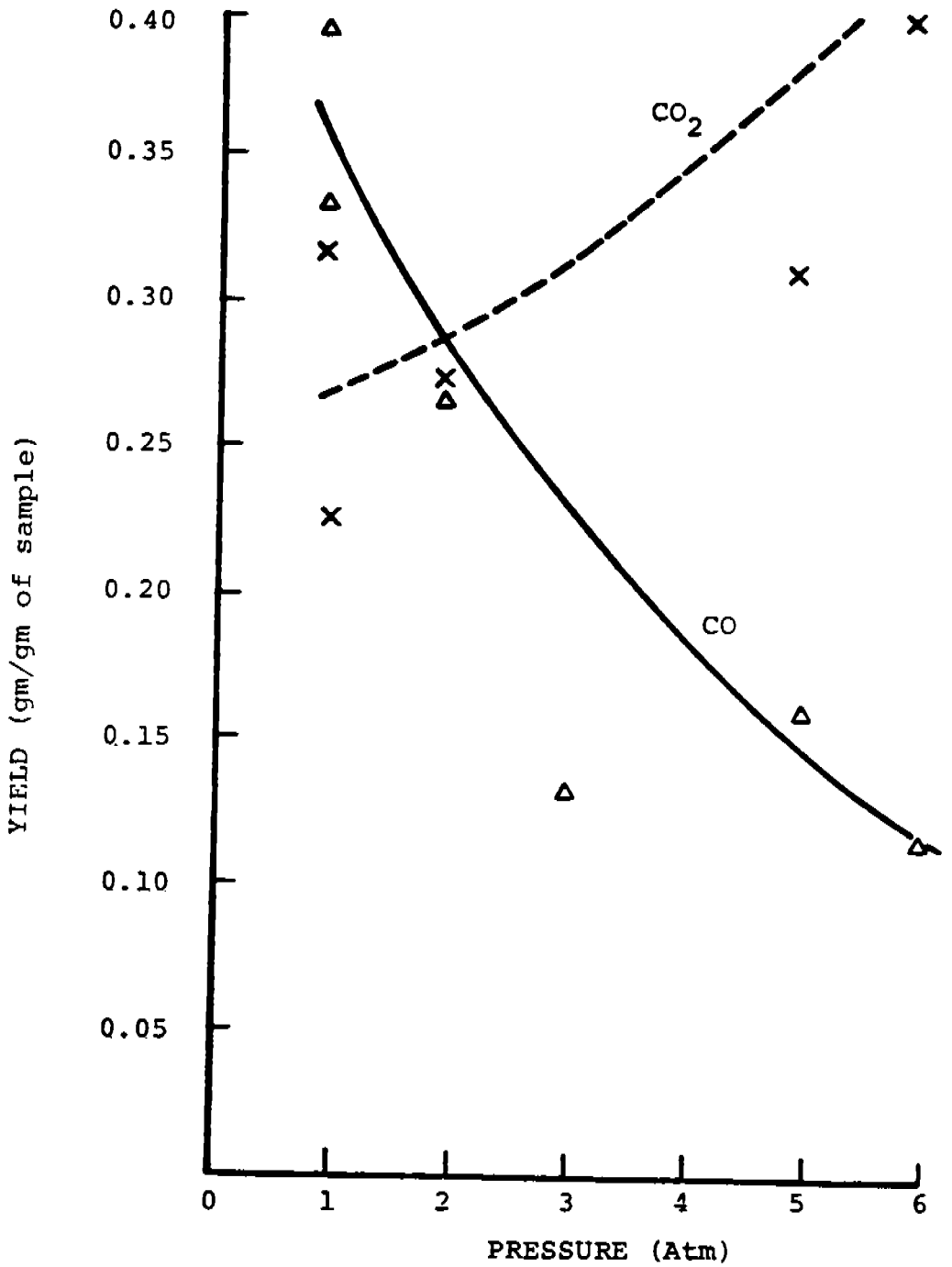

FIGURE 20: YIELD OF CO(Δ) AND CO_2(x) vs PRESSURE

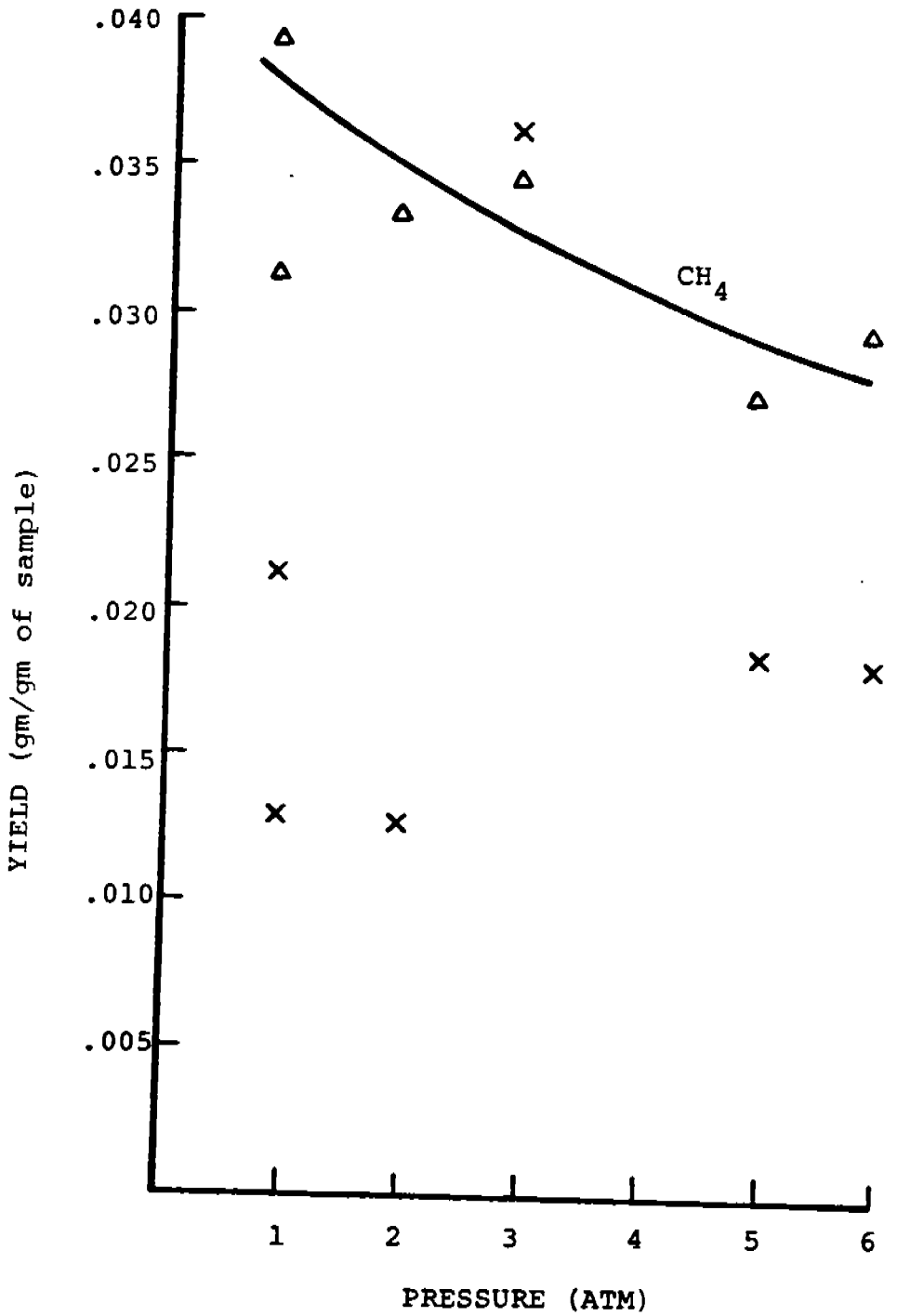

FIGURE 21: YIELD OF CH_4(Δ) AND H_2(x) vs PRESSURE

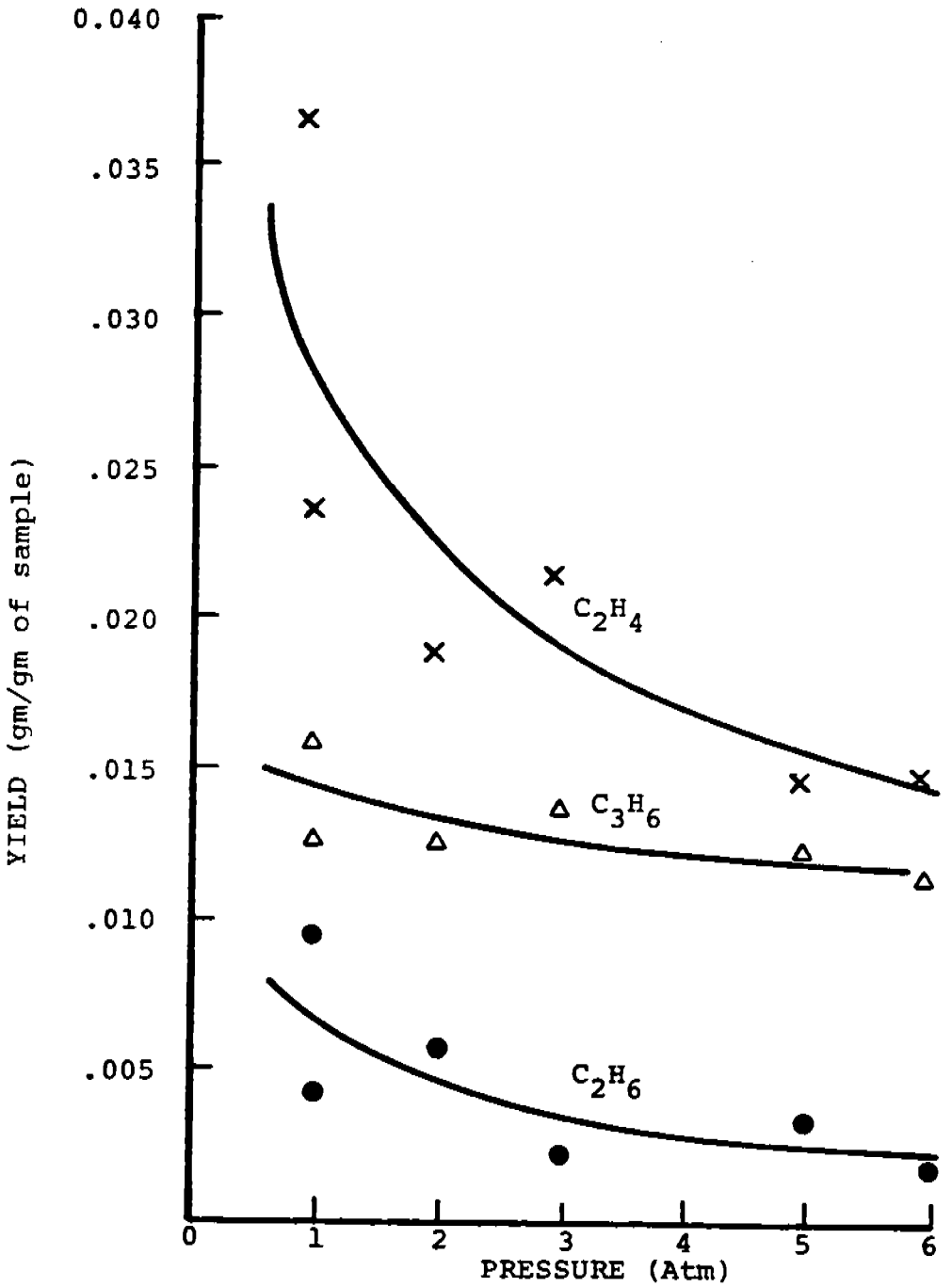

FIGURE 22: YIELDS OF C_2H_4(x), C_3H_6(Δ) AND C_2H_6(•) vs PRESSURE

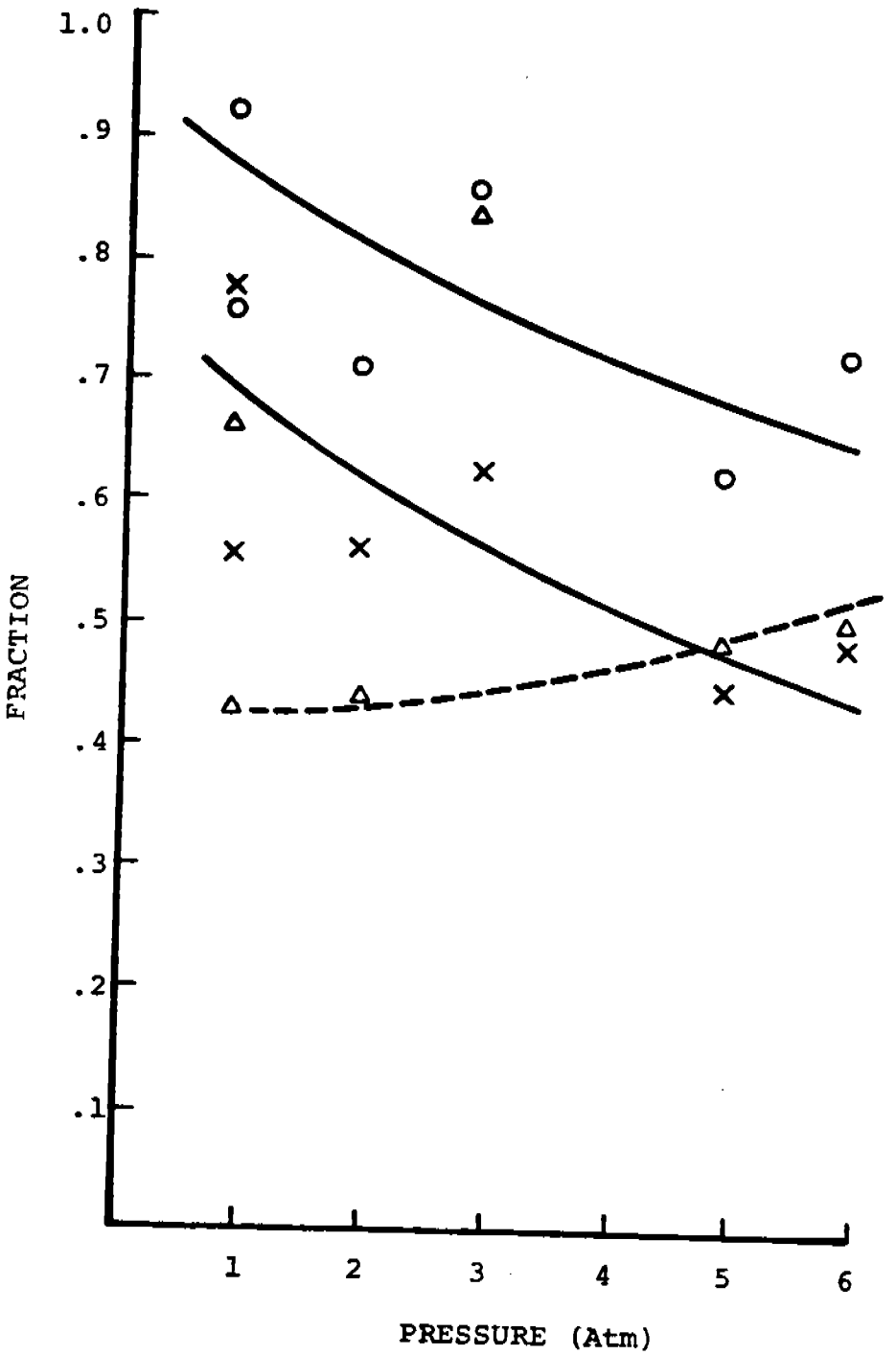

FIGURE 23: FRACTION OF CARBON (x), HYDROGEN (Δ) AND OXYGEN (O) IN GAS vs PRESSURE

that the effect of residence time asymptotes at 1 sec that the residence times of the earlier experiments were chosen. This last experiment was run to check the validity of this assumption.

A comparison of gas yields with 1 and 10 secs residence time at 5 atms is given in Table 2. No gross differences in the yields of H_2, CH_4 and C_2H_4 were detected. However, a drastic decrease in CO is evident, accompanied by a non-negligible increase in C_2H_6 and CO_2, and a decrease in C_3H_6. This is reflected by an increase of carbon fraction and a decrease in oxygen fraction.

The material balances of all the above experiments were somewhat unsatisfactory, averaging only at 0.6. We believe that a loss of char is the explanation for the poor material balance. The Avicel cellulose is an extermely fine powder and the char it forms can easily be blown away from the sample cup, and thus lost. If this were true, then the validity of the gas trends shown can be maintained. To verify this explanation, we used Whatman No. 1 filter paper as a sample. The structural integrity of the sample prevented the char from being blown away. At the same time, the effects of long residence time suggested by the previous experiment could also be verified.

A series of four experiments were performed, with the goals of 1) closing the mass balance, 2) checking the validity of the observation that production of C_2H_6 is favored at the expense of CO production in a system of high pressure and long residence time. The results are summarized in Table 3.

As expected, the structural integrity of the Whatman filter paper prevented the char from being blown away; consequently we were able to collect the char, and close the mass balance. A char yield as high as 22% was collected, and the mass balance obtained was on the order of 85% to 90%. A phenomena not observed previously is a definite increase of char yield due to the low purge gas flow rate and consequent long residence time.

TABLE 2

COMPARISON OF GAS YIELDS* BETWEEN A RESIDENCE TIME OF 1 AND 10 SECONDS. EXPERIMENT CONDUCTED AT 5 ATM

	1 sec	10 sec
CO_2	3.04×10^{-1}	3.55×10^{-1}
CO	1.48×10^{-1}	8.5×10^{-3}
H_2	1.8×10^{-2}	1.40×10^{-2}
CH_4	2.69×10^{-2}	2.81×10^{-2}
C_2H_6	3.13×10^{-3}	1.28×10^{-2}
C_2H_4	1.43×10^{-2}	1.21×10^{-2}
C_3H_6	1.21×10^{-2}	3.49×10^{-3}
$C_{fraction}$	0.442	0.542
$H_{fraction}$	0.482	0.495
$O_{fraction}$	0.618	0.576

* units in $\frac{\text{g in gas}}{\text{g of sample}}$

A longer residence time is shown again to effect a decreased yield of CO and C_3, and an increase in C_2H_6. An increase in CO_2 and a decrease in C_2H_4 is also observed. H_2 and CH_4 formation is apparently not affected by residence time.

3.3 Phase Two Research

This phase consisted of a series of experiments to study the effect of the presence of a small amount of free oxygen on the pyrolysis process. The goal was to identify the conditions that would maximize the yield of CO and H_2, and minimize CO_2 formation. Experiments were conducted at 1 and 5 atm, again using 10 mg samples of Whatman Filter Paper.

To determine a suitable rate of oxygen flow, the time needed for pyrolysis was first calculated. Then the equilibrium product mixture as a function of feed to oxygen ratio was calculated by the NASA thermochemical equilibrium computer program, and the ratio that would yield maximum CO vs CO_2 was determined. Dividing the amount of oxygen needed by the time of pyrolysis, a flow rate of 2 cc per minute was determined.

3.3.1 Procedures (for 5 atm runs).

- Purge reactor, insert sample, keep sample at 150°C.
- Close the reactor outlet valve, but not completely. (open wide for 1 atm runs)
- Set O_2 tank at 80 psig, adjust O_2 restriction valve to achieve desired reactor pressure (60 psig). Then shut off O_2 supply and vent the O_2 flow.
- Adjust steam restriction valve to achieve the same reactor pressure, and let the system stabilize.
- Reopen the O_2 valve.
- By adjusting the reactor outlet valve slightly, calibrate the system for the desired rate of steam (or O_2) flow.
- When all conditions are set, record the flow rates.
- Connect the condenser and collector and start watch 1.

- Wait approximately 10 minutes to let the oxygen purge out any air in the system.
- Heat up sample rapidly.
- Start gas collection at 200°C and start watch 2.
- Turn down sample heater at 500°C and allow to cool down.
- Disconnect condenser and stop both watches. Amount of water condensed will be the H_2O output.
- Analyze gas collected by gas chromatography.
- When sample returns to 150°C, reconnect condenser etc. and repeat the process, heating up, collecting gas, and disconnecting at times identical to the experimental run. Amount of H_2O and O_2 collected will be taken as the H_2O and O_2 input. Their flow rates are also determined.
- Depressurize the system and measure the amount of char collected.

3.3.2 Results. The results are summarized in Table 4, which compares runs at the two different pressures. The same results are compared with previous runs without the additional oxygen input in Table 5. In interpreting the carbon, hydrogen and oxygen fraction present in the gas, and the various material balances, it must be kept in mind that the denominator is the amount contained in the solid sample, not the total material input which would include the free oxygen and the steam. Consequently, it is not surprising to find a very low hydrogen balance, since a large portion is lost through oxidation to water; and an oxygen balance over 100% due to the unaccounted free oxygen input.

The effects of the free oxygen input can be seen in Table 5. It is found that there is an approximate 20% increase in CO_2 yield, 10% increase in CO and a 10% decrease in H_2. The yields of the lower hydrocarbons (CH_4, C_2H_4, C_2H_6) have also decreased while the higher hydrocarbons (C3 and C4's) have been greatly reduced to trace amounts. This clearly indicates a combustion phenomenon, which

TABLE 3

EFFECT OF RESIDENCE TIME ON HIGH PRESSURE
(5 ATM) GAS PHASE PYROLYSIS

	Residence Time	1 sec	3 sec	15 sec	18 sec
Yield	CO_2	3.23×10^{-1}	5.6×10^{-1}	5.79×10^{-1}	4.85×10^{-1}
	H_2	1.80×10^{-2}	2.31×10^{-2}	1.84×10^{-2}	1.1×10^{-2}
	CO	1.67×10^{-1}	9.65×10^{-2}	3.72×10^{-3}	4.22×10^{-3}
	CH_4	3.47×10^{-2}	3.76×10^{-2}	4.04×10^{-2}	3.56×10^{-2}
	C_2H_4	2.24×10^{-2}	2.44×10^{-2}	1.30×10^{-2}	1.42×10^{-2}
	C_2H_6	1.20×10^{-2}	1.65×10^{-2}	2.69×10^{-2}	2.25×10^{-2}
	C_3H_6	1.53×10^{-2}	1.27×10^{-2}	3.12×10^{-3}	4.52×10^{-3}
	C_4H_8	5.69×10^{-3}	4.32×10^{-3}	3.28×10^{-4}	2.96×10^{-3}
Fraction	C	0.523	0.587	0.508	0.445
	H	0.570	0.680	0.584	0.444
	O	0.668	0.871	0.857	0.719
Char		14.71%	16.03%	21.45%	22.87%
Balance	C	0.78	0.87	0.89	0.85
	H	0.66	0.78	0.72	0.59
	O	0.72	0.93	0.93	0.80
Mass		0.74	0.89	0.90	0.81

TABLE 4

RESULTS OF OXYGENATED CELLULOSE PRESSURE AT 1 AND 5 ATM

Yield*	1 atm	5 atm
CO_2	5.08×10^{-1}	4.58×10^{-1}
H_2	1.15×10^{-2}	1.17×10^{-2}
CO	4.59×10^{-1}	2.66×10^{-1}
CH_4	1.88×10^{-2}	2.17×10^{-2}
C_2H_4	1.82×10^{-2}	1.48×10^{-2}
C_2H_6	2.27×10^{-3}	1.51×10^{-3}
C_3H_6	6.06×10^{-3}	6.9×10^{-3}
C_4H_8	9.28×10^{-3}	2.99×10^{-4}
C Fraction	0.832	0.62
H Fraction	0.317	0.332
O Fraction	1.28	0.982
CHAR	9.365%	14.88%
C Balance	0.995	0.88
H Balance	0.375	0.43
O Balance	1.31	1.04
Mass Balance	1.115	0.93

*units in gm in gas/gm of sample

TABLE 5

THE EFFECT OF OXYGEN ON CELLULOSE PYROLYSIS

Yield*	1 Atm w/O_2	1 Atm w/o O_2	5 Atm w/O_2	5 Atm w/o O_2
CO_2	5.08×10^{-1}*	3.16×10^{-1}	4.58×10^{-1}	3.23×10^{-1}
H_2	1.15×10^{-2}	2.11×10^{-2}	1.17×10^{-2}	1.8×10^{-2}
CO	4.59×10^{-1}	3.95×10^{-1}	2.66×10^{-2}	1.67×10^{-1}
CH_4	1.88×10^{-2}	3.94×10^{-2}	2.17×10^{-2}	3.47×10^{-2}
C_2H_4	1.82×10^{-2}	3.66×10^{-2}	1.48×10^{-2}	2.24×10^{-2}
C_2H_6	2.27×10^{-3}	3.38×10^{-2}	1.51×10^{-3}	1.2×10^{-2}
C_3H_6	6.06×10^{-3}	1.58×10^{-2}	6.9×10^{-3}	1.53×10^{-2}
C_4H_8	9.28×10^{-4}	5.37×10^{-3}	2.99×10^{-4}	5.69×10^{-3}
C Fraction	0.832	0.77	0.62	0.52
H Fraction	0.317	0.663	0.332	0.57
O Fraction	1.28	0.922	0.982	0.668
CHAR	9.365%	--**	14.88%	14.71%

* units in gm in gas/gm of sample

** char % not accurate enough for comparison

first breaks down the higher hydrocarbons to lower ones, followed by oxidation to form CO and finally to CO_2. Overall, the fraction of carbon present in the effluent increased by 10%. The oxygen fraction increased by 30% to over 100%, while the hydrogen fraction decreased by 30%. The loss of hydrogen suggests preferential oxidation of the hydrogen to form water. There was no effect on the char yield.

The effect of pressure on pyrolysis in the presence of oxygen can be seen in Table 4. Consistent with results from previous pyrolysis experiments without the oxygen, pressure effects an increase in char yield and a decrease in gas yield. Yields of CO and all hydrocarbons have decreased. However, instead of increasing the yield of CO_2, pressure effects a slight decrease in CO_2 for pyrolysis in the presence of oxygen. No effect on the H_2 yield is observed.

Another interesting observation is the amount of free oxygen consumed. The free oxygen flow rate of approximately 2 ml/min was determined by assuming a pyrolysis time of 1-1/2 min and that maximum CO production would be found in the equilibrium mixture of $C_6H_{10}O_5$ and O_2 if their ratio by weight is 10:4. In other words, with a 10 mg sample, 4 mg of oxygen is expected to be consumed. Assuming the free oxygen takes part only in the gas phase reaction, then by taking the difference of the oxygen fraction in gas between experiments with and without the free oxygen input, one can calculate that .37 and .31 mg of free oxygen was consumed in the 1 and 5 atm runs respectively. In the 1 atm case, the consumption of .37 mg of free O_2 out of the 4 mg available during pyrolysis suggests that almost all available free O_2 was consumed. Further, it is indicated that at higher pressure, less oxygen was consumed. Now, since the null effect on char yield has led to the conclusion that O_2 reacts only within the gas phase, the less volatiles at higher pressure will explain the decrease in O_2 consumption. This is further evidenced by the drop in CO_2 and CO formation.

3.4 Phase Three Research

After the insertion of the micro-reactor into the DSC, a series of experiments followed to study the effects of pressure on the heat of pyrolysis. To allow for cross referencing the results with earlier data, every effort was made to keep the reactor system design similar to the system before the merger with the DSC. The gas phase heating block and the exit valve system was kept intact. The same 10 mg samples of Whatman Filter paper were used. However, argon was used as a carrier in place of steam to allow a higher pressure and easier handling. Steam was not necessary since we were not interested in product collection.

After insertion of the sample, the reactor was set at the desired pressure and flow rate. The DSC was then programmed to heat up the solid phase pyrolysis zone at 5°C per min. A Model 385 Linear 2 pen chart recorder was used to monitor the sample temperature and the DSC output signal, which is a measurement of heat flow (in mW). When the primary zone reached 500°C, it was maintained in an isothermal condition for about 5 to 10 minutes, before ending the experiment. The system was then cooled down to ambient and then reprogrammed up at the same rate, this time with only the char left in the sample pan. This second run provides a base line for comparison with the sample run. A typical output is attached in Figure 24. After cooling down from the base line run, the sample pan was removed and the amount of char recorded.

Before presenting the results, a discussion of the calibration is necessary. Comparing the initial DSC curve with the baseline curve, the point where the sample line diverges from the baseline and the point where it returns are visually determined. A straight line is joined between the two points which encloses an area under the sample curve peak (see dotted line in Figure 24). This area represents the heat of pyrolysis.

FIGURE 24: REPRESENTATIVE DSC CURVE FOR CELLULOSE PYROLYSIS AT 5 ATM

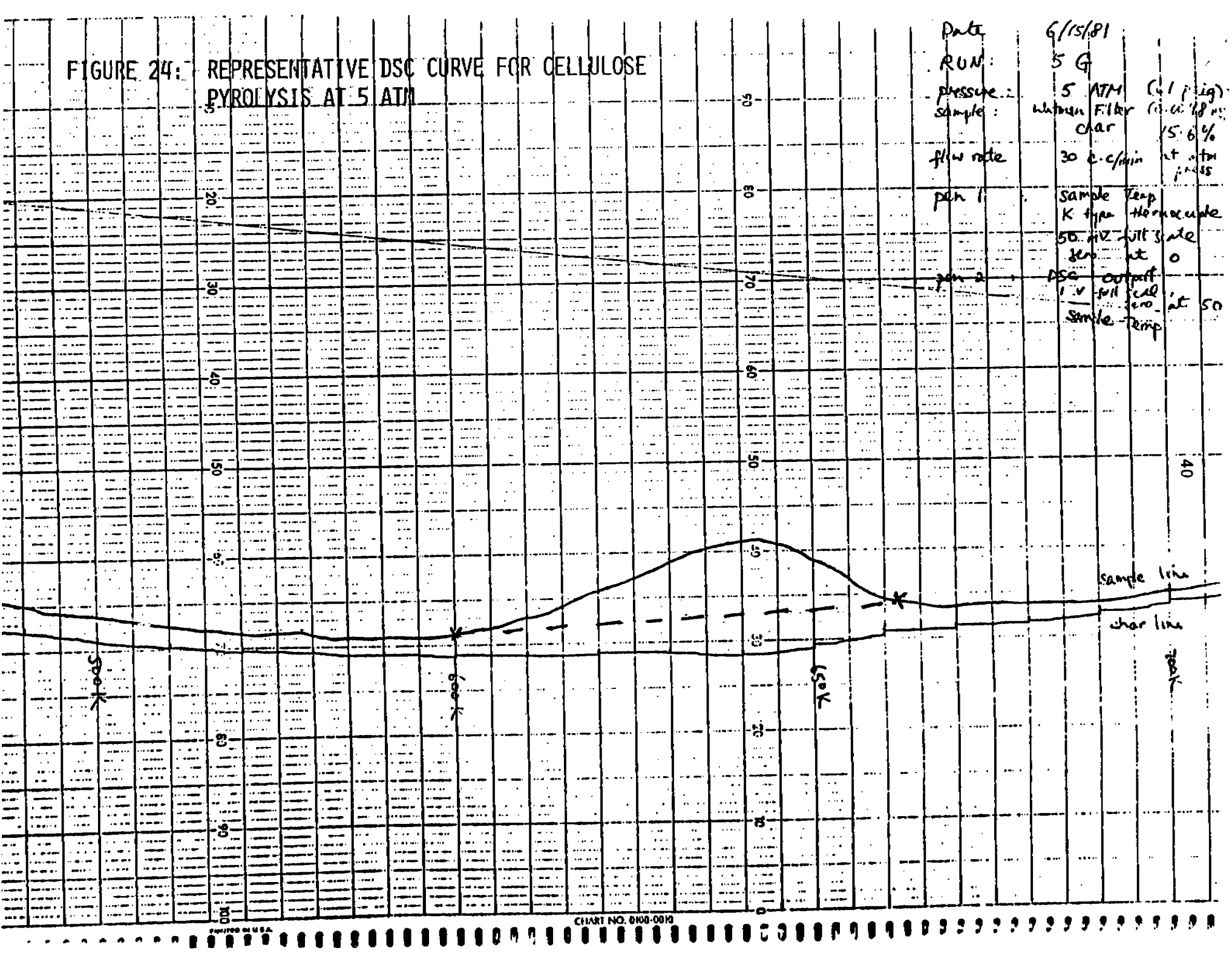

A calibration curve provided by Setaram, which has been shown in this laboratory to be accurate (more discussion later), converts the voltage output on the ordinate to a wattage. The energy needed for pyrolysis is obtained by integrating along the time axis. The heat of pyrolysis is then normalized by the sample size.

The heats of pyrolysis reported here are all based on the Setaram calibration curve provided with the instrument, which assumes use of the DSC in its standard configuration without the micro-reactors. There is reason to believe that after the installation of the metal micro-reactor reactor tubes, with all their external accessories, the response of the DSC may have been affected. Due to the delicacy of the equipment, we are still searching for suitable heat of reaction standards to calibrate the DSC under the present system. The numbers reported here will then be confirmed, or rescaled if necessary. Nevertheless, the trend reported here is believed to be correct.

3.4.1 Results and Discussions. Results of all the experiments are tabulated in Table 6. The initial parameter varied was pressure, the effect of which we intend to study. It was later discovered that the flow rate of the purge gas is a very important hidden parameter. The flow rate was measured by flow meter on the atmospheric side of the exit restriction valve. A simple continuity relationship was used to back calculate the flow velocity inside the reactor. Any turbulence effects caused by flow over the sample cup are assumed to be consistent for all runs. Plotting results of experiments with high and low flow rates separately gives well correlated results. Figure 25 plots the heat of pyrolysis vs. pressure, Figure 26 plots char yield vs. pressure.

These results show that $\Delta H_{pyrolysis}$ decreases with pressure. In particular, a dramatic change from endothermicity to exothermicity is observed with the low flow rate experiments. Accompanying the decrease in the heat of pyrolysis is an increase in char yield. Char yield vs. pressure in high flow experiments are

TABLE 6

EFFECT OF PRESSURE ON HEAT OF CELLULOSE PYROLYSIS

Pressure (psi)	Flow Rate (cc/min)	ΔH (cal/gm) *	CHAR %
15	6	+81	13.7
60	30	+73	15.27
60	4	+25	19.23
76	30	+55	15.6
83	10	-30	21.5
95	10	-51	18.6
120	10	-93	21.9
150	15	-147	21
150	60	+10	18.5

* + endothermic

\- exothermic

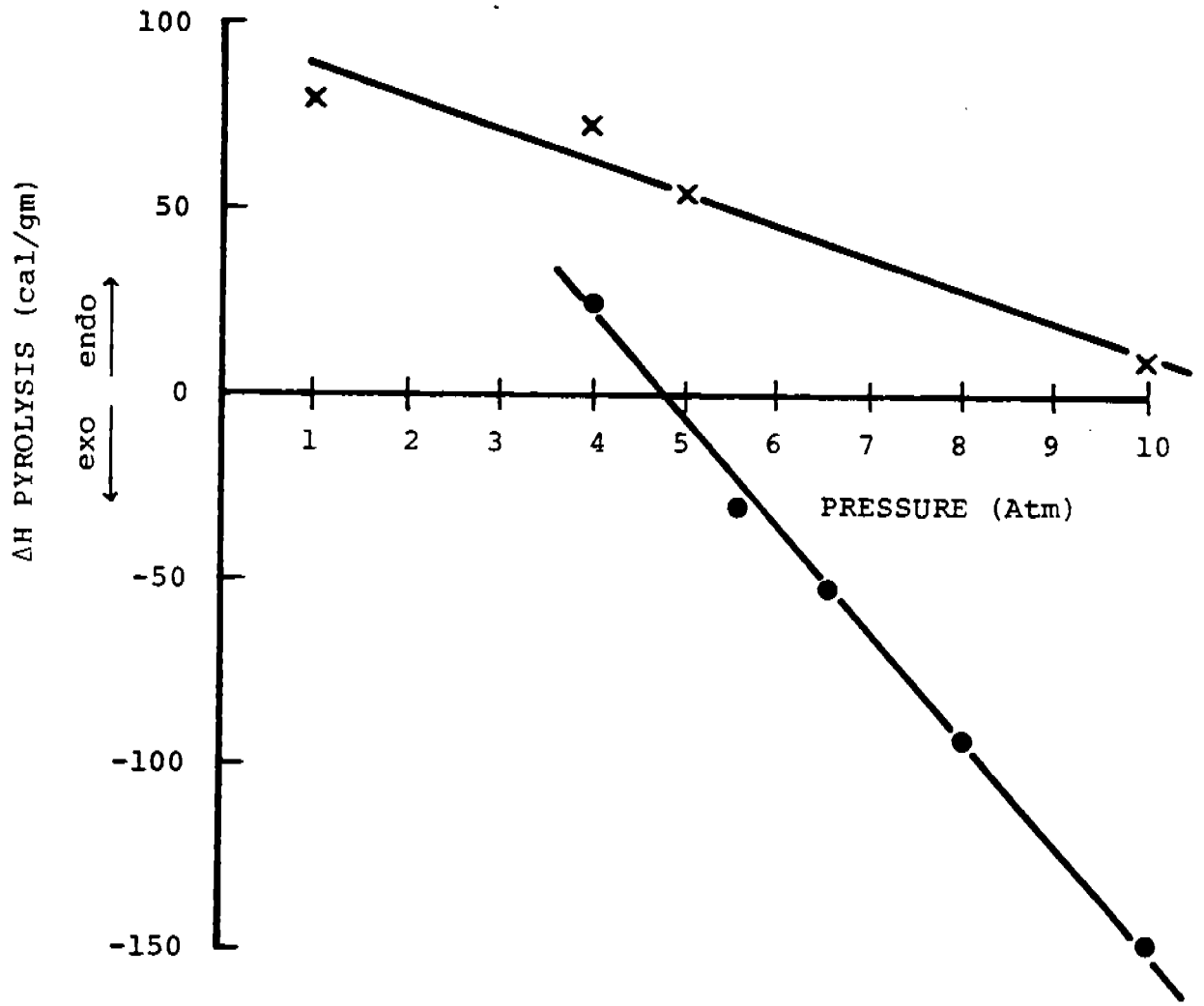

FIGURE 25: PLOT OF ΔH PYROLYSIS vs PRESSURE. EXPERIMENTS CONDUCTED WITH HIGH (x: 0.58 - 0.73 cm/sec) AND LOW PURGE GAS FLOW (●: 0.1 - 0.22 cm/sec) RATES.

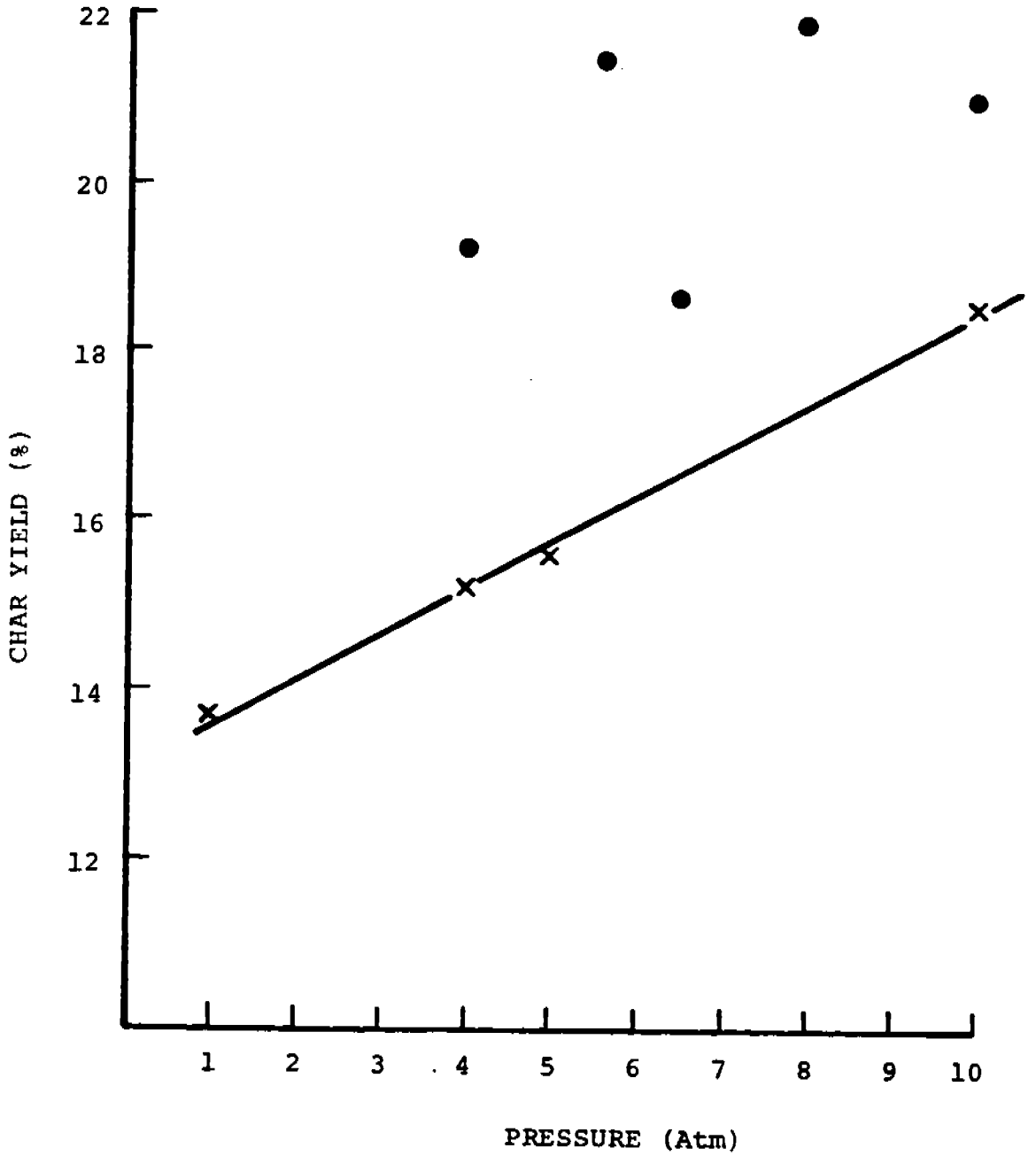

FIGURE 26: PLOT OF CHAR YIELD vs PRESSURE. EXPERIMENTS CONDUCTED AT HIGH (x : 0.58 - 0.75 cm/sec) AND LOW (•: 0.1 - 0.22 cm/sec) PURGE GAS FLOW RATES.

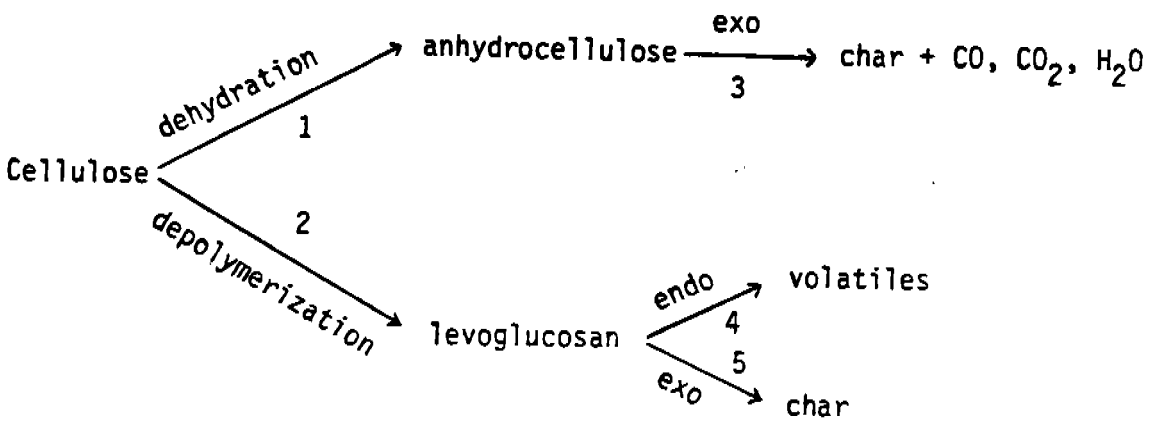

Figure 27: A summary of the cellulose pyrolysis mechanism [based on Arsenau (2)]

well correlated, while those from low flow experiments are not.

These results can be interpreted in light of the pyrolysis mechanism. Cellulose pyrolysis is very complex, involving various competitive and consecutive reactions. Antal (4) provides a review and summary of the mechanism proposed by various workers. The summary is attached in Figure 27. The DSC is capable of seeing into different segments of the scheme of reactions.

First, it is noticed visually from the experiments that there are two types of char. One has a strong structural integrity, retaining the shape of the original sample, while the other type is soft and fluffy. The former is presumed to be the product of reaction 3 (Figure 27), which is not depolymerized; the latter is the result of Step 5. The reaction involved in Step 5 is not agreed upon. Arseneau (5) suggests a decomposition of levoglucosan, but others (6) suggest a repolymerization of volatile matter. The present data suggest that pressure favors both of these char forming exothermic reactions.

With high flow rates, only the residual (first type) char stays in the sample cup, thus allowing complete collection of the residue. The increase yield of residual char shows that pressure favors the dehydration of cellulose to anhydrocellulose over depolymerization to levoglucosan in the competition between Steps 1 and 2. The exothermicity of reaction 3 which follows contributes to a less total heat requirement in pyrolysis, thus a decrease in endothermicity.

With low flow rates, the heat of pyrolysis turns dramatically exothermic, and the char yields are not well correlated. There are two explanations to this phenomena. Arseneau (5) studied the competitive reaction between 4 and 5 and reported that decomposition of levoglucosan to char is favored under mass transfer limiting conditions when the levoglucosan has difficulty escaping and is subjected to further coking. A low flow rate and high pressure would create this situation. This reaction is strongly exothermic, thus explaining the dramatic change in the $\Delta H_{pyrolysis}$. Further, in a low flow situation, an

inconsistent portion of the char from the levoglucosan is trapped in the sample pan, while the rest deposits along the walls of the reactor. This explains the bad correlation of char yield at low flows.

The second explanation is that with a low flow, the DSC is 'seeing' more of the total reaction; whereas at high flow rates, the volatiles formed are quickly swept away from the small DSC sensitive zone, and not reflected in the thermogram. The heat given off by reaction 5 is not recorded, thus the decrease in endothermicity is not as drastic as in the low flow cases. In other words, with a high flow rate, we are seeing only the competition between steps 1 and 2; while with low flow rates, competition between steps 4 and 5 is also visible.

3.5 Conclusions

It is apparent, after one year of experimentation and evaluation, that the reactor system is not well suited for the work of phases 1 and 2, where gas phase reactions are involved. The high surface area to volume ratio of the reactor may have introduced significant wall effects, which inhibits our ability to draw meaningful conclusions regarding the basic gas phase chemistry. Consequently, only certain general observations can be made.

To summarize, it is found that high pressure favors the formation of CO_2 vs. formation of CO and all hydrocarbons. In general, gaseous products have decreased while char formation has increased. A long residence time is observed to have increased formation of C_2H_6 at the expense of CO and C_3's. It also favors formation of char and CO_2. With the addition of oxygen, a combustion phenomena by oxidation to CO and finally to CO_2 is observed. The free oxygen apparently does not participate in the solid phase pyrolysis reaction.

The work of phase 3 is considered successful. Well correlated data is obtained, which agrees well with the cellulose pyrolysis mechanism. It is shown that pressure favors the char forming exothermic reactions.

3.6 Future Work

With the instrumentation and techniques developed in phase 3, one hundred and twenty experiments have been proposed to carefully detail the effects of pressure on biomass pyrolysis. This work will involve various samples of biomass, including cellulose, hemicellulose, lignin and two other materials, employing various heating rates, and at pressures up to 25 atms.

With more data available, more insights can be drawn into the pyrolysis mechanism. Operating conditions which favor the different routes in the scheme of reactions can be identified. Questions arising from the disagreement between various proposed mechanisms can hopefully be answered.

4.0 CONCLUSIONS

The thermal analysis research has shown the method of kinetic analysis by Friedman signatures of weight loss curves holds great promise for detailing complex pyrolytic reaction mechanisms. However, better experimental data derived from Setaram or Mettler instruments should be obtained before extensive mathematical analyses are undertaken.

Results of the exploratory work using the pressurized micro-reactor system were of mixed quality. Continuing research (supported by DOE/Battelle N.W. Laboratories) will focus on the effects of pressure on the pyrolytic heats of reaction of various biomass materials.

5.0 ACKNOWLEDGMENTS

The authors wish to thank Dr. Beverly Berger, and Symon Friedrich with U.S.D.O.E, Drs. Thomas Reed and Thomas Milne with S.E.R.I., and Dr. Don Stevens with Battelle N.W. Laboratories for their interest in this research. The technical assistance of Mr. William E. Edwards with Princeton University is also gratefully acknowledged.

6.0 REFERENCES

1. Antal, M. J., "Thermogravimetric Fingerprints of Complex Solid Phase Pyrolysis Mechanisms and Kinetics," Eastern States Section of The Combustion Institute, Fall Meeting, Oct. 1980.

2. Antal, M. J., "Thermogravimetric Signatures of Complex Solid Phase Pyrolysis Mechanisms and Kinetics," to appear.

3. Urban, D. L. and M. J. Antal, "A Study of the Kinetics of Sewage Sludge Pyrolysis Using DSC and TGA" submitted to FUEL for publication.

4. Antal, M. J., Friedman, H. L. and F. E. Rogers, "Kinetics of Cellulose Pyrolysis in Nitrogen and Steam," Combustion Science and Technology, 1980, Vol. 21, pp. 141-152.

5. Arseneau, D. F., "Competitive Reactions in Thermal Decomposition of Cellulose," Canadian Journal of Chemistry, 49, pp. 632-638.

6. Lewellen, P. C., W. A. Peters, and J. B. Howard, 16th International Symposium on Combustion Proceedings, The Combustion Institute, Pittsburgh, 1977, p. 1471.

APPENDIX A

Thermogravimetric Fingerprints of Complex Solid Phase Pyrolysis Mechanisms and Kinetics

Michael J. Antal, Jr.
Department of Mechanical and Aerospace Engineering
Princeton University
Princeton, New Jersey 08544

Introduction

Pyrolysis plays a critical role in the thermochemical conversion of biomass materials such as wood, agricultural wastes, municipal solid wastes, and various animal wastes, into more useful fuels and chemicals. Pyrolysis also plays an important role in the gasification of coal, the retorting of oil shale, and most combustion processes. Consequently, there is some incentive to develop a better understanding of the detailed pyrolysis chemistry occurring in the thermal environment of conversion reactors, combustors, and related process equipment.

Much effort has been devoted to the study of simple pyrolysis mechanisms governed by the rate equation

$$\frac{dV}{dt} = k(V^*-V)^n \qquad (1)$$

where $V = 1- \frac{w(t)}{w_i}$, $V^* = 1- \frac{w_f}{w_i}$, and $w(t)$ is the time dependent sample weight, w_i the initial sample weight and w_f the final sample weight, k is the Arrhenius rate factor and n the order of the reaction. Usually $k = A \exp(-E/RT)$ where A is the pre-exponential constant, E the activation energy, R the Universal Gas Constant, and T the sample temperature.

Thermogravimetry (TG) is often used to experimentally determine the values of A, E and n for a given material. The kinetic interpretation of thermogravimetry data involves certain mathematical complexities because the sample temperature T is usually chosen to be a linear function of time; thus $T = \alpha+\beta t$. Sestak et al (1) give an excellent review of methods for the kinetic interpretation of thermogravimetric data. Unfortunately, most of the techniques assume that pyrolysis can be characterized as a simple reaction mechanism governed by the rate equation (1). More complex reaction mechanisms have been treated in only a cursory manner. The goal of research described in this paper is to develop a better understanding of complex pyrolysis mechanisms and kinetics through the study of selected model problems. The following sections describe the mathematical models studied to date, the methods of analysis, and early results.

Mathematical Models of Complex Pyrolysis Mechanisms

Table 1 lists various combinations of consecutive and competitive reaction mechanisms which may be used to describe the temperature dependent weight loss of a material undergoing pyrolysis. Parallel independent reactions have been omitted since they are usually associated with heterogeneous materials, whose components could be isolated and studied independently. Although Table 1 only includes mechanisms with up to three steps, its extension to more complex mechanisms is straightforward.

Table 1
A Catalogue of Reaction Mechanisms

Description	Pictorial Representation
One Reaction/Simple	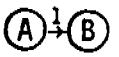
Two Reaction/Competitive	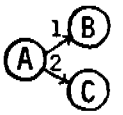
Two Reaction/Consecutive	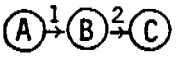
Three Reaction/Competitive	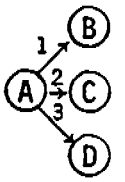
Three Reaction/Consecutive	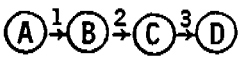
Three Reaction/Competitive-Consecutive	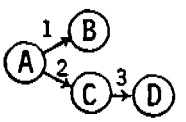
Three Reaction/Consecutive-Competitive	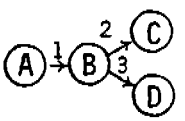

For each of the mechanisms listed in Table 1, the appropriate rate equations describing weight loss as would be measured using thermogravimetry have been written down and solved numerically. For example, the rate equations governing the two reaction/competitive mechanism are

$$\frac{d\rho_A}{dt} = -k_1(\rho_A)^{n_1} - k_2(\rho_A)^{n_2} \qquad (2)$$

$$\frac{d\rho_B}{dt} = s_1\, k_1(\rho_A)^{n_1} \qquad (3)$$

$$\frac{d\rho_C}{dt} = s_2\, k_2(\rho_A)^{n_2} \qquad (4)$$

where ρ_A, ρ_B, and ρ_C are the densities of solid reactant A and solid products B and C, S_1 and S_2 are stoichiometric coefficients giving the fractional weight of solid reactant A remaining as solid products B and C (respectively), and the k_i are rate factors as before. Here it is assumed that the volume of the sample remains constant during pyrolysis, so that the densities of A, B and C are directly related to the sample weight. Future research may modify this assumption by incorporating volume change into the rate equation. Solving Equations (2) - (4) numerically with an assumed linear heating rate produces a simulated TG curve for a material undergoing pyrolysis by the indicated mechanism. The question of interest is to determine whether a set of simulated TG curves at various heating rates provides sufficient information to infer the mechanism and associated rate data which were used to construct the TG curves.

Methods of Analysis

Although many methods are available for the kinetic analysis of TG curves, the author's experience with cellulose pyrolysis (2) lead him to emphasize multiple heating rate methods in this research. These methods are attractive since they naturally synthesize the results of several (perhaps many) experiments. Because they do not assume that a single reaction dominates an entire TG curve, they appear to be especially well suited for dissecting the intricacies of complex pyrolysis mechanisms. As described in the following paragraph, two differential multiple heating rate methods have been used here.

The Friedman multiple heating rate method (3) assumes Equation (1) to be applicable to a set of TG curves spanning a narrow range of heating rates. If the values of $\ln(dV/dt)$ are plotted for various heating rates as a function of $1/T$, where the values of dV/dt are each associated with the same degree of volatilization $V(t)$ (i.e. $V(t)$ is a constant for a set of values (dV/dt)), then a straight line connecting the points has a slope of $-E/R$. Furthermore, if the values of $\ln(dV/dt)$ for various heating rates are plotted as a function of $\ln(V^*-V(t))$, where the values of dV/dt are each associated with the same value of T, then a straight line connecting the points has slope n. Thus a graph of E vs $V(t)$ and n vs T are obtained using the multiple heating rate method of analysis from a set of TG curves spanning several heating rates. These graphs serve as useful "fingerprints" of complex reaction mechanisms since their shape varies according to the prevalent pyrolysis chemistry. Moreover, the values of E and n are often good first guesses for the values of the kinetic parameters associated with the various mechanisms.

Early Results

The multiple heating rate methods of analysis discussed in the preceding section have been applied to the various model problems discussed earlier and fingerprints of the reaction mechanisms have been obtained. Unfortunately, space does not permit an adequate presentation of all the results, which are primarily graphic or pictorial in nature. Results for the two and three reaction consecutive mechanisms are illustrative of the body of data accumulated to date.

For both mechanisms the E vs $V(t)$ plot begins ($V=0$) with E assuming the value of the rate limiting step and remains relatively constant until the end of the reaction ($V=V^*$) when E rapidly sweeps through the values of E associated with the other steps in the reaction sequence. The n vs T curves show more structure but behave similarly, sweeping the values of n present in the mechanism. The values of n tend to be averaged quantities; whereas the values of E more truly reflect the full range of values present in the model problem. The fingerprints obtained to date do not provide sufficient information to distinguish between the two and three reaction consecutive models.

Conclusions

The use of multiple heating rate methods to analyze various model problems has provided TG fingerprints of various pyrolysis mechanisms. The fingerprints furnish useful guidance for the interpretation of complex pyrolysis reaction mechanisms.

Unfortunately, the fingerprints do not appear to be sufficiently unique to provide positive identification of complex pyrolysis mechanisms using TG curves spanning a variety of heating rates. The fingerprints are useful in narrowing the range of potential mechanisms and rate constants. Furthermore, the juxtaposition of data

obtained from TG experiments, the fingerprints discussed here, and results obtained from the intelligent manipulation of various model problems (solved numerically) may suggest definitive experiments which uniquely define the complex reaction sequence prevalent during pyrolysis. Without this interaction of computation and experiment it seems unlikely to the author that a unique mechanistic explanation of complex pyrolysis phenomenon can be found.

References

1. Sestak, J., Satava, V. and Wendtlandt, W., "The Study of Heterogeneous Processes by Thermal Analysis," Thermochim. Acta, 7, 333 (1973).

2. Antal, M. J., Friedman, H. L. and Rogers, F. E., "Kinetics of Cellulose Pyrolysis in Nitrogen and Steam," Comb. Sci. and Tech., 21, 141 (1980).

3. Friedman, H. L., "Kinetics of Thermal Degradation of Char-Forming Plastics from Thermogravimetry," J. Polym. Sci., C6, 183 (1964).